Report

Current Biology

TES-1/Tes and ZYX-1/Zyxin protect junctional actin networks under tension during epidermal morphogenesis in the *C. elegans* embryo

Highlights

- TES-1 and ZYX-1 promote the integrity of actin networks during elongation
- The LIM domains of TES-1 and ZYX-1 are required for normal function and localization
- TES-1 and ZYX-1 are recruited to apical junctions in a tension-dependent manner
- Both TES-1 and ZYX-1 can be recruited to strained actin fibers

Authors

Allison M. Lynch, Yuyun Zhu, Bethany G. Lucas, ..., Jonathan Pettitt, Margaret L. Gardel, Jeff Hardin

Correspondence

jdhardin@wisc.edu

In brief

Cell-cell junctions are vulnerable to damage due to high tension generated during dramatic morphogenetic changes. Lynch et al. show that the LIM-domain-containing repeat proteins TES-1/Tes and ZYX-1/Zyxin are components of a multicellular, tension-sensitive system that stabilizes the junctional actin cytoskeleton during embryonic morphogenesis.

Lynch et al., 2022, Current Biology *32*, 5189–5199
December 5, 2022
https://doi.org/10.1016/j.cub.2022.10.045

CellPress

Current Biology

CellPress

Report

TES-1/Tes and ZYX-1/Zyxin protect junctional actin networks under tension during epidermal morphogenesis in the *C. elegans* embryo

Allison M. Lynch,[1,13] Yuyun Zhu,[1,13] Bethany G. Lucas,[5] Jonathan D. Winkelman,[6] Keliya Bai,[7,11] Sterling C.T. Martin,[2] Samuel Block,[4,12] Mark M. Slabodnick,[8,9] Anjon Audhya,[4] Bob Goldstein,[9] Jonathan Pettitt,[7] Margaret L. Gardel,[6,10] and Jeff Hardin[1,2,3,14,*]

[1]Program in Genetics, University of Wisconsin, Madison, WI 53706, USA
[2]Biophysics Program, University of Wisconsin, Madison, WI 53706, USA
[3]Department of Integrative Biology, University of Wisconsin, Madison, WI 53706, USA
[4]Department of Biomolecular Chemistry, University of Wisconsin, Madison, WI 53706, USA
[5]Department of Biology, Regis University, 3333 Regis Boulevard, Denver, CO 80221, USA
[6]Institute for Biophysical Dynamics, University of Chicago, Chicago, IL 60637, USA
[7]University of Aberdeen, Institute of Medical Sciences, Aberdeen AB25 2ZD, UK
[8]Department of Biology, Knox University, Galesburg, IL 61401, USA
[9]Department of Biology, University of North Carolina at Chapel Hill, Chapel Hill, NC 27599, USA
[10]Department of Physics, James Franck Institute and Pritzker School of Molecular Engineering, University of Chicago, Chicago, IL 60637, USA
[11]Present address: Max-Planck Institute of Molecular Cell Biology and Genetics, Pfotenhauerstrasse 108, 01307 Dresden, Germany
[12]Present address: Koch Institute for Integrative Cancer Research, Massachusetts Institute of Technology, 77 Massachusetts Avenue, Building 76-511, Cambridge, MA 02139, USA
[13]These authors contributed equally
[14]Lead contact
*Correspondence: jdhardin@wisc.edu
https://doi.org/10.1016/j.cub.2022.10.045

SUMMARY

LIM-domain-containing repeat (LCR) proteins are recruited to strained actin filaments within stress fibers in cultured cells,[1–3] but their roles at cell-cell junctions in living organisms have not been extensively studied. Here, we show that the *Caenorhabditis elegans* LCR proteins TES-1/Tes and ZYX-1/Zyxin are recruited to apical junctions during embryonic elongation when junctions are under tension. In genetic backgrounds in which embryonic elongation fails, junctional recruitment is severely compromised. The two proteins display complementary patterns of expression: TES-1 is expressed in lateral (seam) epidermal cells, whereas ZYX-1 is expressed in dorsal and ventral epidermal cells. *tes-1* and *zyx-1* mutant embryos display junctional F-actin defects. The loss of either protein strongly enhances morphogenetic defects in hypomorphic mutant backgrounds for cadherin/catenin complex (CCC) components. The LCR regions of TES-1 and ZYX-1 are recruited to stress fiber strain sites (SFSSs) in cultured vertebrate cells. Together, these data establish TES-1 and ZYX-1 as components of a multicellular, tension-sensitive system that stabilizes the junctional actin cytoskeleton during embryonic morphogenesis.

RESULTS AND DISCUSSION

We previously conducted a genome-wide RNAi screen in a sensitized HMP-1/α-catenin background to identify genes that, when knocked down, enhanced the severity of the *hmp-1(fe4)* phenotype during morphogenesis in *Caenorhabditis elegans* (*C. elegans*) embryos,[4] including a gene on chromosome IV (Video S1). Previously named temporarily assigned gene 224 (TAG-224), we renamed the protein TES-1 given its significant homology to vertebrate Tes. ClustalW analysis indicated that TES-1 is approximately 35% identical and 64% similar to human Tes. Pfam analysis showed that both proteins have an N-terminal Prickle, Espinas, Testin (PET) domain followed by three C-terminal Lin-I1, Isl-1, Mec-3 (LIM) domains (Figure 1A).

TES-1 is an F-actin-binding protein that functionally interacts with *hmp-1/α-catenin* at the *C. elegans* apical junction

100% of *hmp-1(fe4); tes-1(RNAi)* embryos arrested during the elongation stage of morphogenesis with junctional actin defects (Figures 1B–1E). *tes-1(ok1036); hmp-1(fe4)* double homozygotes similarly exhibit 93.8% lethality and elongation arrest (n = 516 embryos examined), and *tes-1* RNAi enhanced lethality in a *hmp-2/β-catenin* hypomorph (*hmp-2(qm39)*; Figure S1). *Tes-1* RNAi exacerbated junctional-proximal actin defects in *hmp-1(fe4)* homozygotes (Figures 1F–1H). In 26% of *hmp-1(fe4); tes-1(RNAi)* embryos (6 of 23 embryos examined via 4D microscopy), cells leaked out of the ventral midline, compared with 0% of *hmp-1(fe4)* homozygotes (0 of 22 embryos

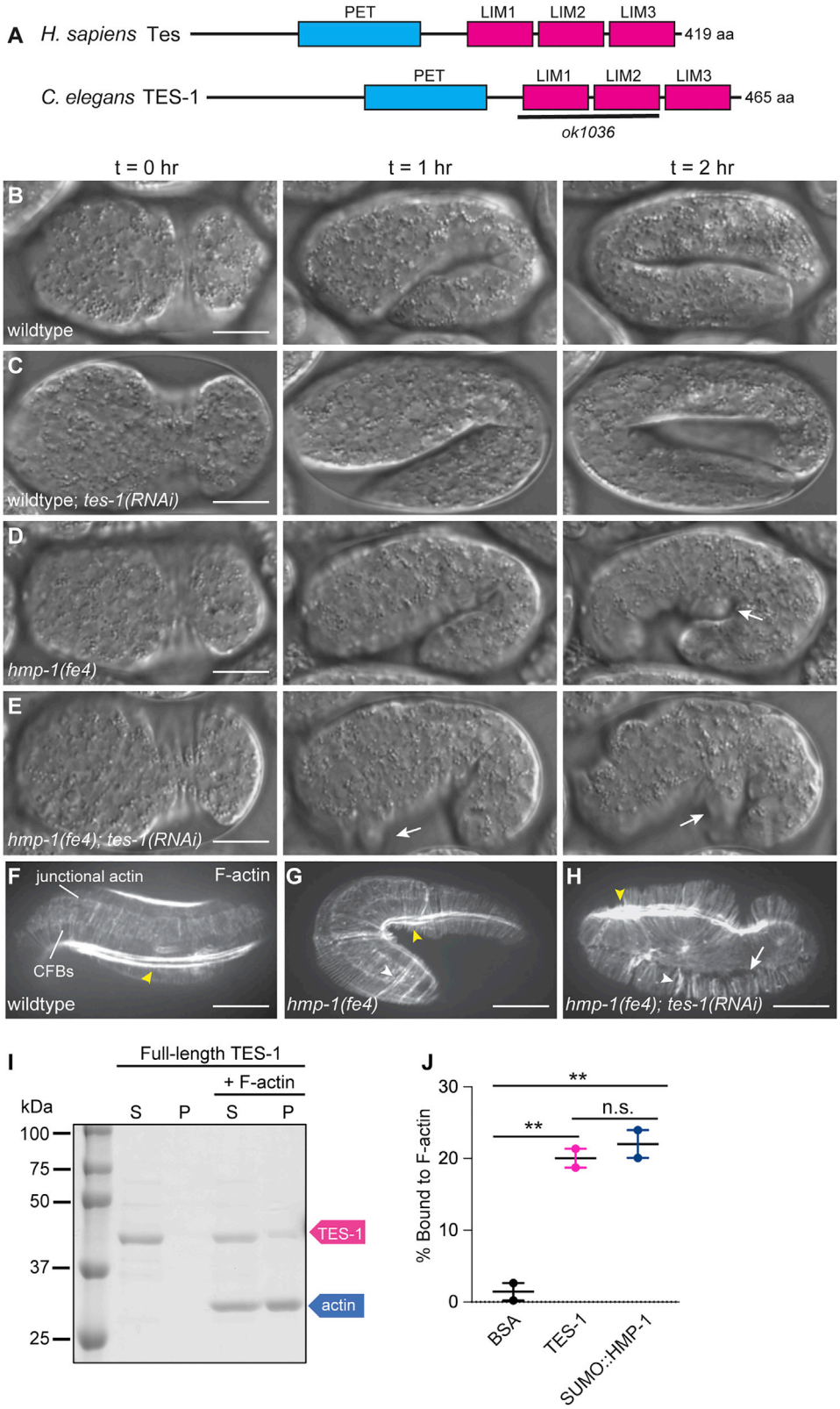

(legend on next page)

examined; significantly different, Fisher's exact test, p = 0.02). Ventral enclosure involves the formation of cadherin-catenin complex (CCC)-dependent junctions at the ventral midline,[5] suggesting that TES-1 is also involved in this process (Figure 1E, arrow). Like vertebrate Tes,[6,7] recombinant TES-1 cosediments with F-actin (Figure 1I) to an extent statistically indistinguishable from HMP-1/α-catenin[8] (Figure 1J).

TES-1 localizes to apical junctions in the embryonic epidermis

We constructed an endogenously tagged version of *tes-1*; *mNG::tes-1* embryos, larvae, and adults that were phenotypically indistinguishable from wild type (Figure 2A). In larvae, TES-1 was visible at alae, epidermal structures produced by seam cells, and in adults, TES-1 was expressed in vulval tissues (data not shown). In early embryos, mNG::TES-1 was visible in the cytoplasm of epidermal cells, and at the 2-fold stage of elongation, mNG::TES-1 puncta began to accumulate at sites of cell-cell contact, expanding and becoming more evenly distributed along cell borders as elongation continued. Strikingly, mNG::TES-1 was maintained at seam-dorsal and seam-ventral but not seam-seam borders (Figure 2B, arrow).

We next performed knockdown of junctional components in *mNG::tes-1* embryos. In *hmr-1(RNAi)* embryos, TES-1::GFP failed to accumulate at junctions (Figure 2C). By contrast, *ajm-1(RNAi)* did not prevent the junctional localization of mNG::TES-1 (Figure 2D); however, TES-1 foci did not spread to form a continuous, intense band as in wild type, which may reflect the failure of *ajm-1(RNAi)* embryos to elongate fully.

Endogenously tagged HMP-1/α-catenin::mScarletI and mNG::TES-1 displayed substantial overlap in embryos (Figure 2E; Pearson's R value above threshold = 0.58, n = 10 junctions), whereas there was little to no overlap with DLG-1/Discs large::dsRed, which localizes basal to the CCC (Figure 2F; R = 0.25, n = 10 junctions; significantly different, p < 0.0001, unpaired Student's t test). Partial localization of Tes with the CCC has similarly been reported in cultured vertebrate cells.[9] Although one study reported that vertebrate α-catenin and Tes can be coimmunoprecipitated,[10] we were unable to replicate this result with *C. elegans* CCC components in a generalized proteomics screen[11] or in directed coIP experiments (Figures S2A and S2B), suggesting that the interaction of TES-1 with the *C. elegans* CCC is indirect. Alternatively, force-dependent interactions between LIM domain-containing repeat (LCR) proteins and cell-cell junctions may be transient and weak, as suggested by a recent BioID study of zyxin,[12] and thus difficult to demonstrate using traditional biochemical approaches.

We reasoned that TES-1 could stabilize CCC-dependent junctional-proximal actin networks during morphogenesis, and so we compared F-actin in *tes-1(ok1036)* homozygous embryos wild type for *hmp-1* with fully wild-type embryos (Figures 2G–2I). Unlike wild-type embryos (Figure 2G), most *tes-1(ok1036)* embryos displayed significantly narrower zones of junctional-proximal actin (Figure 2H; quantified in Figure 2J), as well as more severe phenotypes, including gaps between circumferential filament bundles (CFBs), CFB collapse, and the complete loss of preserved junctional-proximal actin (Figure 2I; quantified in Figure 2K). We conclude that TES-1 stabilizes junctional-proximal actin during morphogenesis.

TES-1 requires its PET and LIM domains

To identify functionally important subdomains of TES-1, we analyzed endogenously tagged *tes-1* deletions. Unlike full-length mNG::TES-1 (Figure 3A), mNG::TES-1ΔPET localized along all seam cell borders in the epidermis (Figure 3B). mNG::TES-1ΔLIM1-3 localized along structures that appear to be CFBs (Figure 3C). This result suggests that the latent ability of TES-1 to bind to CFBs is not normally manifest when the N terminus is present and is similar to vertebrate Tes, which can co-immunoprecipitate actin[7] and localize via its N terminus in a non-mechanosensitive manner.[10,13,14] Line scans indicated that when either the PET or LCR domains were deleted, TES-1 still localized to seam-dorsal and seam-ventral junctions (Figure 3D), but embryos showed ectopic TES-1 junctional localization at seam-seam junctions (Figure 3E). Deletion of the PET domain led to an increase in junctional versus cytoplasmic signal compared with wild type, whereas the removal of all three LIM domains resulted in the opposite effect (Figure 3F). It is possible that the PET and LCR domains interact, restricting their domain-specific binding affinities, as has been proposed for vertebrate

Figure 1. TES-1 loss enhances phenotypes in hypomorphic CCC backgrounds

(A) Protein domain maps of *C. elegans* TES-1 and human Tes. TES-1 and Tes both contain N-terminal Prickle, Espinas, and Testin (PET) domains and three C-terminal Lin-11, Isl-1, and Mec-3 (LIM) domains. The *tes-1(ok1036)* allele removes LIM1-2 along with some intronic sequence and introduces a frameshift into the remainder of the coding region.

(B–E) *tes-1(RNAi)* enhances the severity of morphogenetic defects in *hmp-1(fe4)* embryos.

(B) Wild-type embryo imaged using Nomarski microscopy.

(C) *tes-1(RNAi)* embryo.

(D) *hmp-1(fe4)* embryo; bulges become apparent during embryonic elongation (t = 2 h).

(E) In *hmp-1(fe4); tes-1(RNAi)* embryos, cells leak out of the ventral midline (t = 1 h), and all embryos die with severe elongation defects (t = 2 h). Scale bars, 10 μm.

(F–H) *tes-1(RNAi)* enhances the severity of actin defects in *hmp-1(fe4)* embryos. Phalloidin staining of wild-type (F), *hmp-1(fe4)* (G), and *hmp-1(fe4); tes-1(RNAi)* (H) embryos. The bright signal is muscle (yellow arrowheads). Wild-type embryos maintain a population of junctional-proximal actin along cell borders, and dorsal and ventral epidermal cells in elongated embryos contain circumferential actin filament bundles (CFBs) that are evenly spaced. *hmp-1(fe4)* embryos also typically maintain junctional-proximal actin; however, their CFBs are less evenly spaced and sometimes clump together (white arrowhead). *hmp-1(fe4); tes-1(RNAi)* embryos display clumping of CFBs (white arrowhead) and a complete lack of junctional-proximal actin. CFBs appear to have been torn away from the junction, leaving bare zones devoid of F-actin (white arrow). Scale bars, 10 μm.

(I) TES-1 binds to F-actin in an actin co-sedimentation assay. Full-length TES-1 remains in the supernatant fraction (S) when incubated without F-actin. However, TES-1 is detected in the pellet fraction (P) when incubated with 5 μM F-actin.

(J) Quantification of TES-1 found in the pellet after incubation with F-actin. Bovine serum albumin (BSA) served as a negative control and SUMO::HMP-1 as a positive control. TES-1 bound to F-actin significantly more than BSA did (two replicates; **p < 0.01, unpaired Student's t test).

See also Figure S1 and Video S1.

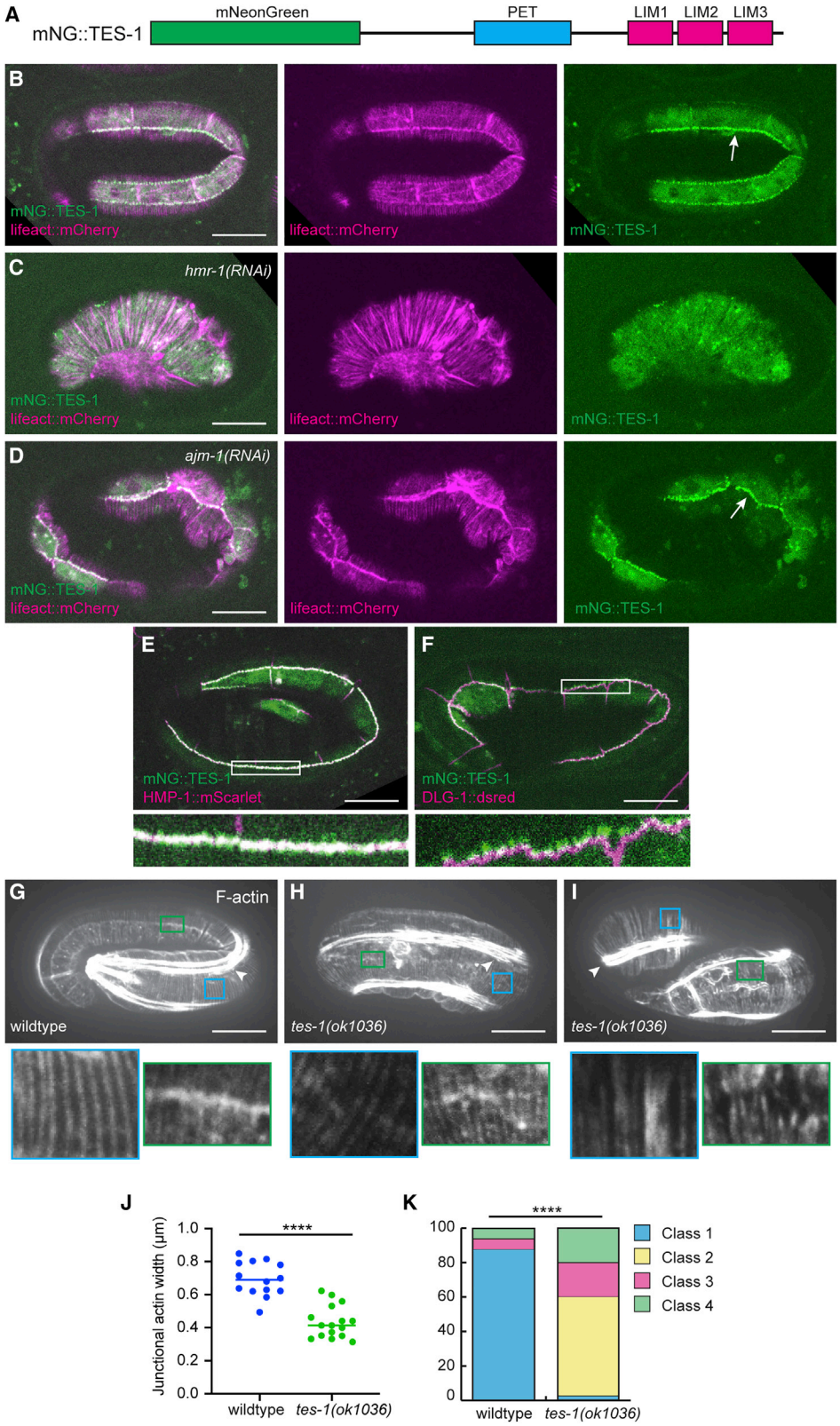

Figure 2. TES-1 localizes to sites of cell-cell attachment during embryonic elongation

(A) A schematic of the endogenous mNG::TES-1 knockin strain used in this study.

(B) mNG::TES-1 localizes strongly to seam-dorsal and seam-ventral boundaries (arrow).

(legend continued on next page)

Tes based on biochemical assays.[7] These results indicate that both the LCR and PET domains are required for normal levels and sites of TES-1 junctional recruitment.

We also expressed various TES-1::GFP deletion constructs (Figure S3A) in transgenic embryos. Full-length TES-1::GFP, TES-1ΔPET::GFP, and TES-1ΔLIM1-3 recapitulated the expression of endogenous knockins (Figures S3B–S3D). TES-1::GFP rescued lethality in *tes-1(ok1036)/+; hmp-1(fe4)* embryos. *tes-1(ok1036)/+; hmp-1(fe4)* worms exhibited 80% lethality (n = 20 embryos scored); the addition of extrachromosomal TES-1::GFP reduced lethality to 38% (n = 92 embryos scored). *tes-1(ok1036); hmp-1(fe4)* worms could develop to adulthood but only if they expressed *tes-1::gfp*, indicating the TES-1::GFP is functional. The deletion of LIM1 (Figure S3E) or LIM2 (Figure S3F) led to sporadic recruitment to epidermal junctions, including some seam-seam junctions, and what appear to be actin-containing structures in epidermal cells. The deletion of LIM3 rendered TES-1::GFP largely cytoplasmic (Figure S3G).

Due to maternal effects and gonadal defects, assessing synergistic lethality of *tes-1::gfp* deletion constructs in *tes-1(ok1036); hmp-1(fe4)* homozygous mothers proved challenging. Fertile *tes-1(ok1036); hmp-1(fe4)* worms harboring *tes-1ΔLIM1::GFP* could not be obtained, and occasional *tes-1(ok1036); hmp-1(fe4)/+; tes-1ΔLIM1::GFP* embryos were able to grow to adulthood but were sterile. Wetherefore tested for the ability of TES-1::GFP fragments to rescue synergistic lethality in *tes-1(ok1036); hmp-1(fe4)/+* embryos (Figure S3H). TES-1ΔPET::GFP significantly rescued some embryonic lethality in this genetic background, but progeny displayed germline malformations, protruding vulvae, and sterility. TES-1ΔLIM1-3::GFP, TES-1ΔLIM2::GFP, and TES-1ΔLIM2::GFP were unable to rescue the 39% lethality observed among the progeny of *tes-1(ok1036); hmp-1(fe4)/+* mothers. Overall, these results indicate that the LIM domains of TES-1 are crucial for *tes-1* function during morphogenesis.

The difference in localization pattern of TES-1ΔLIM3::GFP and TES-1ΔLIM1-3::GFP was curious since the entire LCR region, with appropriate spacing between LIM domains, has been suggested to be crucial for F-actin binding.[2,3] It has been suggested, however, that the LIM1-2 domain of vertebrate Tes can engage in both heterophilic binding to proteins such as zyxin and homodimerization via interaction with the PET domain of Tes.[10] Although it is not currently known if homodimeric Tes is sequestered away from cell-cell adhesion sites, the deletion of LIM3 could favor such homodimerization. Alternatively, the deletion of LIM3 may cause misfolding of the truncated protein.

TES-1 localizes to junctions in a tension-dependent manner

Tes is required for the maintenance of stress fibers in cultured vertebrate cells,[15] accumulates at focal adherens junctions (AJs) (spot-like foci of cell-cell adhesion) in human vascular endothelial cells,[9] and accumulates at stress fibers downstream of Rho signaling.[14] These data suggest that Tes might play tension-dependent roles in stabilizing F-actin networks at AJs during morphogenesis. A coordinated change in the shape of epidermal cells drives elongation of the *C. elegans* embryo to approximately 4-fold its original length[16] during which contractile forces result in elevated tension specifically at seam-ventral and seam-dorsal junctions.[5,17–20] Given the localization of TES-1, we sought to test whether it is recruited to junctions in a tension-sensitive manner during embryonic elongation.

Because *hmr-1/cadherin*, *hmp-1/α-catenin*, and *hmp-2/β-catenin* homozygous null mutant embryos fail to progress past the 2-fold stage of elongation, we could not assess whether the disruption of TES-1::GFP recruitment to junctions is due primarily to physical absence of CCC components or to the pre-elongation death of the embryos. We therefore examined *hmp-1(fe4)* embryos expressing TES-1::GFP. Although some *hmp-1(fe4)* embryos failed to elongate appreciably, other embryos extended to the 2-fold stage of elongation. TES-1::GFP did not localize to junctions in *hmp-1(fe4)* embryos that failed to elongate past 1.5-fold (10 of 10 embryos; Figures 3G and 3J), even in embryos that survived and hatched. However, TES-1::GFP did localize to junctions in the rare *hmp-1(fe4)* embryos that elongated to at least 2-fold their original length (5 of 5 embryos examined; significantly different; Fisher's exact test, $p = 0.0003$; Figure S3I). The correlation between the extent of elongation of *fe4* embryos and TES-1::GFP junctional recruitment suggests that TES-1 is recruited to junctions in cells that generate sufficient tension to elongate to the 2-fold stage.

We next introduced the full-length TES-1::GFP into *let-502(sb118ts)/Rho kinase* worms to reduce actomyosin contractility in the epidermis (Figures 3H, S3K, and S3L). When *let-502(sb118ts); tes-1::gfp* embryos were imaged at the permissive temperature, TES-1::GFP localized to junctions normally (Figure S3K; quantified in Figure 3J, *let-502(sb118ts)* $\geq$ 1.5×). At the restrictive temperature (25°C), however, TES-1::GFP

(C) *hmr-1(RNAi)* completely prevents mNG::TES-1 localization at junctions.
(D) *ajm-1(RNAi)* does not influence the ability of mNG::TES-1 to localize to junctions (arrow). Scale bars, 10 μm.
(E) mNG::TES-1 co-localizes with endogenous HMP-1::mScarletI.
(F) mNG::TES-1 does not co-localize with DLG-1::dsRed.
Insets in (E) and (F) show magnifications of boxed regions. Scale bars, 10 μm.
(G–I) Fixed and phalloidin-stained embryos. Bright staining is muscle (arrowhead). Scale bars, 10 μm.
(G) Wild-type embryos exhibit parallel circumferential filament bundles (CFBs, blue box inset) and retain junctional-proximal actin (green box inset).
(H) Approximately half of *tes-1(ok1036)* embryos exhibit reduced junctional-proximal actin, although CFB organization looks normal.
(I) *tes-1(ok1036)* embryos also exhibit more severe phenotypes, including gaps and clumping of CFBs (blue box) and a complete loss of junctional-proximal actin (green box).
(J) Width of junctional-proximal actin at seam-non-seam boundaries measured from phalloidin-stained specimens (wild type, n = 14 junctions; *tes-1(ok1036)*, n = 16 junctions; ****$p < 0.0001$, unpaired Student's t test).
(K) Quantification of phalloidin staining phenotypes. Class 1 embryos have normal CFBs and junctional-proximal actin. Class 2 embryos have reduced junctional-proximal actin. Class 3 embryos have reduced junctional-proximal actin and CFB organization defects and class 4 embryos have no retained junctional-proximal actin and CFB organization defects (wild type, n = 16 embryos; *tes-1(ok1036)*, n = 40 embryos; ****$p < 0.0001$, Freeman-Halton extension to Fisher's exact test).
See also Figure S2.

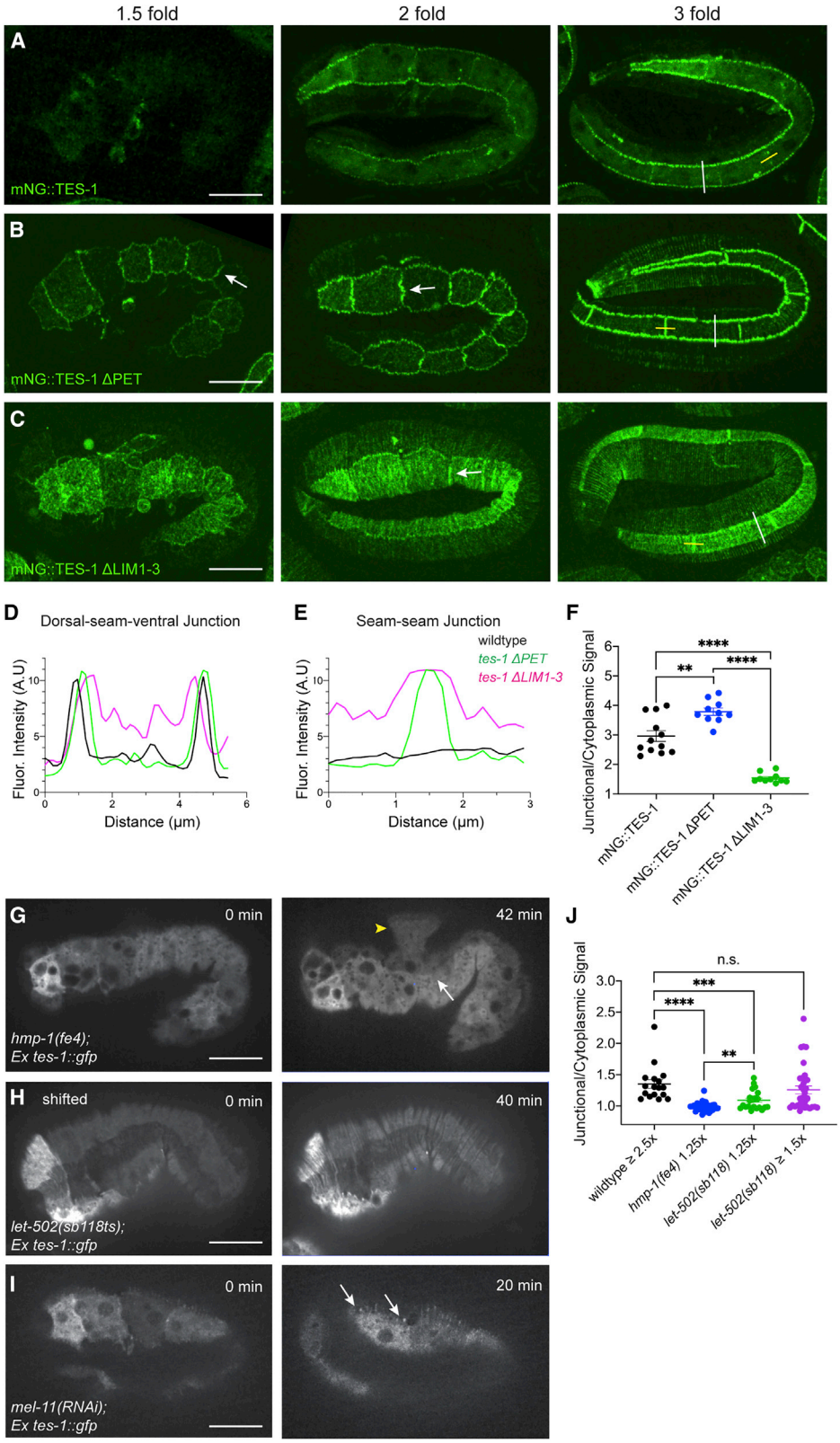

(legend on next page)

remained entirely cytoplasmic in embryos that failed to elongate (Figure 3H; quantified in Figure 3J, *let-502 (sb118)* 1.25×). We also attempted the converse experiment by knocking down MEL-11/myosin phosphatase, which is known to result in excessive epidermal contractility.[18,19] However, adhesion complexes underwent changes in morphology that made this experiment difficult to interpret: the initially continuous distribution of junctional TES-1::GFP was progressively lost, as TES-1::GFP became fragmented and pulled into puncta (Figure 3I). One possibility consistent with this result is that excessive tension leads to the collapse of junctional-proximal actin around CFB insertion sites, including associated TES-1.

ZYX-1/zyxin localizes to junctions in a tension-dependent manner complementary to TES-1

Studies in vertebrate tissue culture cells indicate similar, but not entirely overlapping, localization of Tes and zyxin at spot AJs.[9,21] Moreover, targeted interaction studies[7] and proteomics screens[10] suggest that the two proteins may physically associate, either directly or as part of a complex. We used an endogenous mNG::ZYX-1a knockin[22] (hereafter, ZYX-1) to assess *zyx-1* expression in *C. elegans* embryos. ZYX-1 had been reported to localize at muscle attachment sites[23,24] and sites of cell-cell contact in gastrulating embryos.[22] However, its localization at AJs in the embryonic epidermis had not been reported. ZYX-1 showed strong localization at seam-dorsal and seam-ventral junctions in the epidermis during mid-late elongation. Strikingly, however, ZYX-1 showed a pattern complementary to that of TES-1: whereas mNG::TES-1 showed strong expression in seam cells, ZYX-1 was expressed strongly within non-seam cells (Figure 4A).

Like mNG::ZYX-1, epidermally expressed transgenic ZYX-1::GFP colocalized with the CCC, and its localization was disrupted by HMP-1 depletion (Figures S4A–S4C). Since the LCR domain of zyxin is thought to be required for interaction with F-actin,[2,3] we created an endogenously tagged ΔLIM1-3 strain. mNG::ZYX-1ΔLIM1-3 was much more weakly recruited to junctions (Figure 4B; for quantification, see Figure S4E). We found that loss of *zyx-1* function enhanced the lethality of *hmp-1(fe4)* homozygotes to 100%. This enhancement could be rescued with ZYX-1::GFP expressed under the control of an epidermal-specific promotor, suggesting that its key role is in this tissue (Figure S4D). We next stably expressed GFP-tagged, truncated forms of ZYX-1 in epidermal cells. ZYX-1ΔLIM1-3::GFP was unable to rescue (Figure S4D). Intriguingly, however, a construct lacking LIM1 and LIM3 could very weakly rescue when overexpressed in the epidermis, suggesting a more stringent requirement for the middle of the LCR during morphogenesis. *hmp-1(fe4); zyx-1(gk190)* embryos could not be rescued by epidermal ZYX-1::GFP lacking the N terminus (Figure S4D), indicating a role for the N terminus that is yet to be elucidated. Like mNG::TES-1, mNG::ZYX-1 was much more weakly recruited to seam/non-seam junctions in *let-502(RNAi)* embryos (Figure 4C; for quantification, see Figure S4E). Junctional F-actin defects in *zyx-1(gk190)* homozygotes were more subtle than those in *tes-1(ok1036)* homozygotes (see Figures 2G–2K): we did not detect effects on CFBs but did observe small ruptures in the junctional-proximal actin network at seam-dorsal and seam-ventral boundaries in the embryonic epidermis not observable in controls (Figures S4F–S4H).

Both TES-1 and ZYX-1 can be recruited to strained actin fibers

Mammalian LIM domain proteins are recruited to strained actin fibers via their LIM domain-containing region.[2,3,25] The recruitment of the LCRs of such proteins to stress fiber strain sites (SFSSs) can be induced by laser irradiation in cultured mammalian cells.[2] We tested whether the LCRs of TES-1 and ZYX-1 behave similarly. When transfected into mouse embryonic fibroblasts (MEFs), ZYX-1(LIM1-3)::mCherry was recruited to SFSSs with kinetics similar to the LCR of full-length, eGFP-tagged *M. musculus* zyxin (Figure 4D; quantified in Figures 4E and 4H; for a movie of the entire cell, see Video S2). Compared with full-length *M. musculus* GFP-zyxin, the recruitment of the TES-1 LCR was less pronounced

Figure 3. TES-1 localization requires its PET and LCR domains

For relevant domains of TES-1, see Figure 1A.

(A) Full-length endogenous mNG::TES-1 localizes to dorsal-seam and ventral-seam cell boundaries in the epidermis prominently by the 2-fold stage.

(B) Unlike full-length mNG::TES-1, mNG::TES-1ΔPET localizes along all seam cell borders in the epidermis, including seam-seam borders (arrows). There is also localization at what appear to be actin-containing structures in epidermal cells.

(C) Deletion of LIM1-3 perturbs junctional localization: mNG::TES-1ΔLIM1-3 localizes sporadically to epidermal junctions, including seam-seam junctions (arrow). However, there is also localization to actin networks in seam cells and along structures that appear to be CFBs in non-seam cells. Scale bars, 10 μm.

(D and E) Line scans of mNG::TES-1 signal across dorsal-seam and ventral-seam cell boundaries (D; the position of scans indicated by the white lines in A–C) and seam-seam boundaries (E; yellow lines in A–C) for full-length (WT) *mNG::tes-1*, *mNG::tes-1ΔPET*, and *mNG:: ΔLIM1-3* embryos.

(F) Junctional/cytoplasmic signal for mNG::TES-1 (n = 12 junctions), mNG::TES-1ΔPET (n = 10), and mNG::TES-1ΔLIM1-3 (n = 10). $^{**}p < 0.01$, $^{****}p < 0.0001$, unpaired Student's t test.

(G–I) TES-1::GFP localization in elongation-defective transgenic embryos expressing TES-1::GFP.

(G) In *hmp-1(fe4)* embryos that do not elongate past 1.5-fold before failing, TES-1::GFP does not localize to junctions and instead remains entirely cytoplasmic (arrow). The yellow arrowhead indicates the characteristic Humpback phenotype. See Figure S3I for images of *fe4* embryos that partially elongate.

(H) In *let-502(sb118ts); tes-1::gfp* embryos reared at the restrictive temperature ("shifted"), LET-502 protein is inactivated, embryos fail to elongate, and TES-1::GFP never accumulates along epidermal junctions. Unshifted embryos display normal development and TES-1::GFP localizes to junctions as in wild type (Figure S3K).

(I) In *mel-11(RNAi); tes-1::gfp* embryos, TES-1::GFP is pulled away from junctions in long extensions from epidermal cell borders. In embryos that elongate normally TES-1::GFP junctional localization is not affected (not shown). Scale bars, 10 μm.

(J) Junctional/cytoplasmic ratio of TES-1::GFP in wild-type embryos at ≥2.5-fold stage of elongation (n = 17 junctions), *hmp-1(fe4)* embryos at 1.25-fold stage of elongation (n = 32), and *let-502(RNAi)* embryos at 1.25× (n = 23) and ≥1.5× (n = 33) stages of elongation. $^{**}p < 0.01$, $^{***}p < 0.001$, $^{****}p < 0.0001$, unpaired Student's t test.

See also Figure S3.

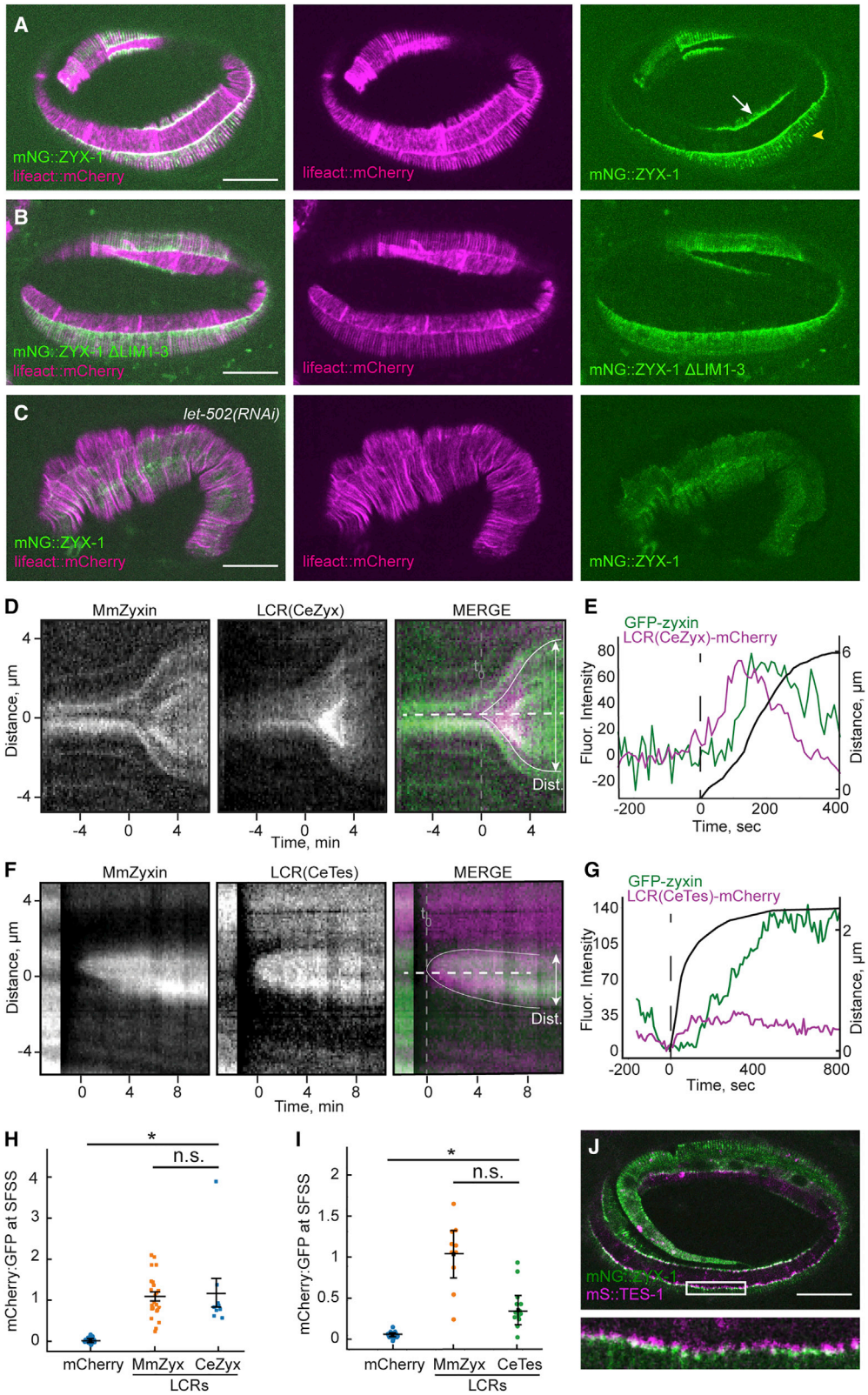

Figure 4. ZYX-1 is also recruited to junctions during elongation and both ZYX-1 and TES-1 are recruited to strained actin filaments

(A) mNG::ZYX-1 is recruited to both dorsal-seam and seam-ventral junctions (white arrow), and it also co-localizes with CFBs after the 2-fold stage (yellow arrowhead).

(legend continued on next page)

but significant compared with the mCherry negative control (Figure 4F; quantified in Figures 4G and 4I; also see Video S3).

ZYX-1/zyxin and TES-1/Tes act largely independently during elongation

We next assessed the interdependence of TES-1 and ZYX-1 in the epidermis during embryonic elongation. Endogenously tagged TES-1 and ZYX-1 appeared to abut one another across cell-cell junctions (Figure 4J), and they did not co-localize quantitatively at junctions (Pearson's R above threshold = 0.0, 13 junctions measured). We saw no change in the localization of mNG::TES-1 to specific boundaries at the 3- to 4-fold stage in *zyx-1(gk190)* or *zyx-1 null* (*cp419*)[22] homozygotes (Figures S4I–S4K), nor did we see mislocalization of mNG::ZYX-1 in *tes-1(ok1036)* homozygotes (Figures S4L and S4M). We did not see any obvious enhancement of lethality in *tes-1; zyx-1* double loss-of-function embryos, but occasional *tes-1(syb5622); zyx-1(cp419)* animals showed minor body morphology defects that became less severe during larval molts (3 out of 30 embryos). Finally, based on previous studies of vertebrate homologs,[7,26] we assessed the physical interaction of TES-1 and ZYX-1. Although we were able to co-immunoprecipitate TES-1 and ZYX-1 (Figures S2C and S2D), we were only able to detect a very weak, substoichiometric interaction between TES-1 and ZYX-1 via the pull-down of bacterially expressed proteins (Figure S2D).

In summary, our results suggest that two LCR proteins—ZYX-1 in non-seam cells and TES-1 in seam cells—act largely independently to bolster cadherin-dependent connections to the junctional-proximal F-actin network during embryonic elongation. A similar division of labor between these two cell types has been elegantly demonstrated previously in the case of non-muscle myosin and other proteins in a series of investigations.[20,27–29] Our results are consistent with experiments in vertebrates, which show that although the depletion of zyxin can reduce the amount of Tes at focal adhesions,[7] Tes can still localize independently of zyxin.[26] Our results further suggest that the loss of one of these LCR proteins in an otherwise wild-type background in *C. elegans* is insufficient to decrease tension below the threshold required for recruitment of the other in the complementary group of epidermal cells.

The TES-1 LCR showed less avid recruitment to SFSSs than the ZYX-1 LCR when expressed heterologously. A previous study in tissue culture cells suggested that a crucial phenylalanine (F66) is found in the LIM domains of proteins that show mechanosensitive recruitment to SFSSs.[3] Notably, zyxin has the F66 feature, but Tes does not.[2,3] There may be assay dependence regarding this requirement, however, as F66 is not required for recruitment of isolated LCR domains to SFSSs.[2] Moreover, Tes has recently been shown to be activated by Rho signaling,[14] and since Rho activity is upregulated in seam cells during embryonic elongation in *C. elegans*,[27,30] the activation of TES-1 in these cells could result in less functional difference in activity of TES-1 and ZYX-1 *in vivo*. Whether ZYX-1 and TES-1 play subtly different roles at the subcellular level is an interesting avenue for future investigation.

Elongating epidermal cells in the *C. elegans* embryo are likely to be subject to "self-injury," as they must remodel their junctional-proximal actin networks to undergo dramatic changes in shape. Our previous experiments indicated that UNC-94/tropomodulin is recruited to junctions under tension, where it presumably protects minus ends of F-actin filaments from subunit loss.[31] Our current results are consistent with a model in which actomyosin-mediated tension generated in elongating embryos leads to strain-dependent recruitment of TES-1 and ZYX-1 to these same junctions during elongation, stabilizing strained junctional actin filaments against the rigors of mechanical stress during morphogenesis.

STAR★METHODS

Detailed methods are provided in the online version of this paper and include the following:

- KEY RESOURCES TABLE
- RESOURCE AVAILABILITY
  - Lead contact
  - Materials availability
  - Data and code availability
- EXPERIMENTAL MODEL AND SUBJECT DETAILS
- METHOD DETAILS
  - Molecular cloning
  - CRISPR
  - Microinjection
  - Antibody and phalloidin staining
  - DIC Imaging
  - Confocal microscopy
  - Colocalization analysis
  - Protein expression and purification
  - Actin-Pelleting assays
  - Co-immunoprecipitations and western blots

(B) In *mNG::zyx-1ΔLIM1-3* embryos ZYX-1 is largely absent from junctions and is not recruited to CFBs.
(C) *let-502(RNAi)* embryos partially lose junctional localization of mNG::ZYX-1. Scale bars, 10 μm. (D–I) Recruitment of TES-1 LCR::mCherry and ZYX-1 LCR::mCherry to stress fiber strain sites (SFSSs) in transfected mouse embryonic fibroblasts.
(D) Representative kymographs of laser-induced recruitment of the ZYX-1 LCR::mCherry and mouse GFP::Zyxin to SFSSs. For a time-lapse sequence of the entire cell, see Video S2. The white dashed and gray solid lines indicate where fluorescence and distance were measured. The dashed gray vertical line indicates t_0, when strain is first observed.
(E) Quantification of GFP and mCherry accumulation over time in the kymograph from (D).
(F) Representative kymographs of laser-induced recruitment of TES-1 LCR::mCherry and mouse GFP::Zyxin to SFSS. For a time-lapse sequence of the entire cell, see Video S3.
(G) Quantification of GFP and mCherry accumulation over time in the kymograph from (F).
(H and I) Intensity of *C. elegans* ZYX-1 LCR::mCherry (H) and *C. elegans* TES-1 LCR::mCherry (I) relative to full-length mouse GFP::Zyxin present in the same cells. Blue dots in each graph represent mCherry alone relative to GFP::MmZyx. TES-1 LCR::mCherry accumulates markedly ($p = 0.023$, $n > 10$; unpaired Student's t test) but to a lesser extent than MmZyx; error bars indicate 95% confidence intervals.
(J) mNG::ZYX-1 does not co-localize with mScarletI::TES-1. The inset shows the magnification of the boxed region. Scale bars, 10 μm.
See also Figures S2 and S4 and Videos S2 and S3.

- Stress fiber strain site assay
- QUANTIFICATION AND STATISTICAL ANALYSIS

SUPPLEMENTAL INFORMATION

Supplemental information can be found online at https://doi.org/10.1016/j.cub.2022.10.045.

ACKNOWLEDGMENTS

cDNA clones for *hmr-1*, *ajm-1*, *zyx-1*, *zoo-1*, *hmp-1*, and *tes-1* (yk collection) were provided by Yuji Kohara (National Institute of Genetics). A.M.L., Y.Z., B.G.L., S.C.T.M., and J.H. were supported by NIH grant R01GM058038 and NIH MIRA R35GM145312 awarded to J.H.; S.C.T.M. was supported by a Gilliam Fellowship from the Howard Hughes Medical Institute and by an Advanced Opportunities Fellowship and a COVID-19 dissertation completion fellowship from the University of Wisconsin-Madison; S.B. and A.A. were supported by NIH MIRA R35GM134865 awarded to A.A.; J.D.W. was supported by NIH grant F32GM122372 and by NIH grant R01GM104032 and the Army Research Office Multidisciplinary University Research Initiative W911NF1410403 awarded to M.L.G.; and B.G. and M.M.S. were supported by NIH MIRA R35GM134838 awarded to B.G. and NIH grant F32GM119348 awarded to M.M.S. Some strains were provided by the *Caenorhabditis* Genetics Center (CGC; https://cbs.umn.edu/cgc/home), which is funded by the NIH Office of Research Infrastructure Programs (P40 OD010440).

AUTHOR CONTRIBUTIONS

A.M.L., Y.Z., J.P., and J.H. conceived and designed the experiments. A.M.L., Y.Z., and J.H. interpreted the data. A.M.L., Y.Z., B.G.L., J.D.W., K.B., S.C.T.M., S.B., and M.M.S. performed the experiments and provided the strains. A.A., B.G., J.P., M.L.G., and J.H. provided supervision and support. A.M.L., B.G.L., Y.Z., and J.H. wrote the manuscript with input from the other authors.

DECLARATION OF INTERESTS

The authors declare no competing interests.

Received: June 8, 2022
Revised: September 12, 2022
Accepted: October 19, 2022
Published: November 15, 2022

REFERENCES

1. Smith, M.A., Hoffman, L.M., and Beckerle, M.C. (2014). LIM proteins in actin cytoskeleton mechanoresponse. Trends Cell Biol. *24*, 575–583. https://doi.org/10.1016/j.tcb.2014.04.009.
2. Winkelman, J.D., Anderson, C.A., Suarez, C., Kovar, D.R., and Gardel, M.L. (2020). Evolutionarily diverse LIM domain-containing proteins bind stressed actin filaments through a conserved mechanism. Proc. Natl. Acad. Sci. USA *117*, 25532–25542. https://doi.org/10.1073/pnas.2004656117.
3. Sun, X., Phua, D.Y.Z., Axiotakis, L., Jr., Smith, M.A., Blankman, E., Gong, R., Cail, R.C., Espinosa de Los Reyes, S., Beckerle, M.C., Waterman, C.M., et al. (2020). Mechanosensing through direct binding of tensed F-actin by LIM domains. Dev. Cell *55*, 468–482.e7. https://doi.org/10.1016/j.devcel.2020.09.022.
4. Lynch, A.M., Grana, T., Cox-Paulson, E., Couthier, A., Cameron, M., Chin-Sang, I., Pettitt, J., and Hardin, J. (2012). A genome-wide functional screen shows MAGI-1 is an L1CAM-dependent stabilizer of apical junctions in *C. elegans*. Curr. Biol. *22*, 1891–1899. https://doi.org/10.1016/j.cub.2012.08.024.
5. Costa, M., Raich, W., Agbunag, C., Leung, B., Hardin, J., and Priess, J.R. (1998). A putative catenin-cadherin system mediates morphogenesis of the *Caenorhabditis elegans* embryo. J. Cell Biol. *141*, 297–308.
6. Coutts, A.S., MacKenzie, E., Griffith, E., and Black, D.M. (2003). TES is a novel focal adhesion protein with a role in cell spreading. J. Cell Sci. *116*, 897–906.
7. Garvalov, B.K., Higgins, T.E., Sutherland, J.D., Zettl, M., Scaplehorn, N., Köcher, T., Piddini, E., Griffiths, G., and Way, M. (2003). The conformational state of Tes regulates its zyxin-dependent recruitment to focal adhesions. J. Cell Biol. *161*, 33–39. https://doi.org/10.1083/jcb.200211015.
8. Kang, H., Bang, I., Weis, W.I., and Choi, H.J. (2016). Purification, crystallization and initial crystallographic analysis of the α-catenin homologue HMP-1 from *Caenorhabditis elegans*. Acta Crystallogr. F Struct. Biol. Commun. *72*, 234–239. https://doi.org/10.1107/S2053230X16001862.
9. Oldenburg, J., van der Krogt, G., Twiss, F., Bongaarts, A., Habani, Y., Slotman, J.A., Houtsmuller, A., Huveneers, S., and de Rooij, J. (2015). VASP, zyxin and TES are tension-dependent members of focal adherens junctions independent of the α-catenin-vinculin module. Sci. Rep. *5*, 17225. https://doi.org/10.1038/srep17225.
10. Sala, S., Van Troys, M., Medves, S., Catillon, M., Timmerman, E., Staes, A., Schaffner-Reckinger, E., Gevaert, K., and Ampe, C. (2017). Expanding the interactome of TES by exploiting TES modules with different subcellular localizations. J. Proteome Res. *16*, 2054–2071. https://doi.org/10.1021/acs.jproteome.7b00034.
11. Callaci, S., Morrison, K., Shao, X., Schuh, A.L., Wang, Y., Yates, J.R., Hardin, J., and Audhya, A. (2015). Phosphoregulation of the C. elegans cadherin-catenin complex. Biochem. J. *472*, 339–352. https://doi.org/10.1042/BJ20150410.
12. Cheah, J.S., Jacobs, K.A., Lai, T.W., Caballelo, R., Yee, J.L., Ueda, S., Heinrich, V., and Yamada, S. (2021). Spatial proximity of proteins surrounding zyxin under force-bearing conditions. Mol. Biol. Cell *32*, 1221–1228. https://doi.org/10.1091/mbc.E19-10-0568.
13. Sala, S., Catillon, M., Hadzic, E., Schaffner-Reckinger, E., Van Troys, M., and Ampe, C. (2017). The PET and LIM1-2 domains of testin contribute to intramolecular and homodimeric interactions. PLoS One *12*, e0177879. https://doi.org/10.1371/journal.pone.0177879.
14. Sala, S., and Oakes, P.W. (2021). Stress fiber strain recognition by the LIM protein testin is cryptic and mediated by RhoA. Mol. Biol. Cell *32*, 1758–1771. https://doi.org/10.1091/mbc.E21-03-0156.
15. Griffith, E., Coutts, A.S., and Black, D.M. (2005). RNAi knockdown of the focal adhesion protein TES reveals its role in actin stress fibre organisation. Cell Motil. Cytoskeleton *60*, 140–152. https://doi.org/10.1002/cm.20052.
16. Priess, J.R., and Hirsh, D.I. (1986). Caenorhabditis elegans morphogenesis: the role of the cytoskeleton in elongation of the embryo. Dev. Biol. *117*, 156–173.
17. Piekny, A.J., Johnson, J.L., Cham, G.D., and Mains, P.E. (2003). The Caenorhabditis elegans nonmuscle myosin genes nmy-1 and nmy-2 function as redundant components of the let-502/Rho-binding kinase and mel-11/myosin phosphatase pathway during embryonic morphogenesis. Development *130*, 5695–5704. https://doi.org/10.1242/dev.00807.
18. Wissmann, A., Ingles, J., and Mains, P.E. (1999). The *Caenorhabditis elegans* mel-11 myosin phosphatase regulatory subunit affects tissue contraction in the somatic gonad and the embryonic epidermis and genetically interacts with the Rac signaling pathway. Dev. Biol. *209*, 111–127. https://doi.org/10.1006/dbio.1999.9242.
19. Wissmann, A., Ingles, J., McGhee, J.D., and Mains, P.E. (1997). *Caenorhabditis elegans* LET-502 is related to Rho-binding kinases and human myotonic dystrophy kinase and interacts genetically with a homolog of the regulatory subunit of smooth muscle myosin phosphatase to affect cell shape. Genes Dev. *11*, 409–422.
20. Vuong-Brender, T.T., Ben Amar, M., Pontabry, J., and Labouesse, M. (2017). The interplay of stiffness and force anisotropies drives embryo elongation. eLife *6*, e23866. https://doi.org/10.7554/eLife.23866.
21. Vasioukhin, V., Bauer, C., Yin, M., and Fuchs, E. (2000). Directed actin polymerization is the driving force for epithelial cell-cell adhesion. Cell *100*, 209–219.

22. Slabodnick, M.M., Tintori, S.C., Prakash, M., Higgins, C.D., Chen, A.H., Cupp, T.D., Wong, T., Bowie, E., Jug, F., and Goldstein, B. (2022). Afadin and zyxin contribute to coupling between cell junctions and contractile actomyosin networks during apical constriction. Preprint at bioRxiv. https://doi.org/10.1101/2022.07.04.498649.

23. Lecroisey, C., Martin, E., Mariol, M.C., Granger, L., Schwab, Y., Labouesse, M., Ségalat, L., and Gieseler, K. (2008). DYC-1, a protein functionally linked to dystrophin in Caenorhabditis elegans is associated with the dense body, where it interacts with the muscle LIM domain protein ZYX-1. Mol. Biol. Cell *19*, 785–796. https://doi.org/10.1091/mbc.E07-05-0497.

24. Smith, P., Leung-Chiu, W.M., Montgomery, R., Orsborn, A., Kuznicki, K., Gressman-Coberly, E., Mutapcic, L., and Bennett, K. (2002). The GLH proteins, Caenorhabditis elegans P granule components, associate with CSN-5 and KGB-1, proteins necessary for fertility, and with ZYX-1, a predicted cytoskeletal protein. Dev. Biol. *251*, 333–347.

25. Smith, M.A., Blankman, E., Gardel, M.L., Luettjohann, L., Waterman, C.M., and Beckerle, M.C. (2010). A zyxin-mediated mechanism for actin stress fiber maintenance and repair. Dev. Cell *19*, 365–376. https://doi.org/10.1016/j.devcel.2010.08.008.

26. Hadzic, E., Catillon, M., Halavatyi, A., Medves, S., Van Troys, M., Moes, M., Baird, M.A., Davidson, M.W., Schaffner-Reckinger, E., Ampe, C., et al. (2015). Delineating the Tes interaction site in zyxin and studying cellular effects of its disruption. PLoS One *10*, e0140511. https://doi.org/10.1371/journal.pone.0140511.

27. Diogon, M., Wissler, F., Quintin, S., Nagamatsu, Y., Sookhareea, S., Landmann, F., Hutter, H., Vitale, N., and Labouesse, M. (2007). The RhoGAP RGA-2 and LET-502/ROCK achieve a balance of actomyosin-dependent forces in *C. elegans* epidermis to control morphogenesis. Development *134*, 2469–2479. https://doi.org/10.1242/dev.005074.

28. Gally, C., Wissler, F., Zahreddine, H., Quintin, S., Landmann, F., and Labouesse, M. (2009). Myosin II regulation during *C. elegans* embryonic elongation: LET-502/ROCK, MRCK-1 and PAK-1, three kinases with different roles. Development *136*, 3109–3119. https://doi.org/10.1242/dev.039412.

29. Zhang, H., Landmann, F., Zahreddine, H., Rodriguez, D., Koch, M., and Labouesse, M. (2011). A tension-induced mechanotransduction pathway promotes epithelial morphogenesis. Nature *471*, 99–103. https://doi.org/10.1038/nature09765.

30. Chan, B.G., Rocheleau, S.K., Smit, R.B., and Mains, P.E. (2015). The Rho guanine exchange factor RHGF-2 acts through the Rho-binding kinase LET-502 to mediate embryonic elongation in C. elegans. Dev. Biol. *405*, 250–259. https://doi.org/10.1016/j.ydbio.2015.07.010.

31. Cox-Paulson, E.A., Walck-Shannon, E., Lynch, A.M., Yamashiro, S., Zaidel-Bar, R., Eno, C.C., Ono, S., and Hardin, J. (2012). Tropomodulin protects alpha-catenin-dependent junctional-actin networks under stress during epithelial morphogenesis. Curr. Biol. *22*, 1500–1505. https://doi.org/10.1016/j.cub.2012.06.025.

32. Lecroisey, C., Brouilly, N., Qadota, H., Mariol, M.C., Rochette, N.C., Martin, E., Benian, G.M., Ségalat, L., Mounier, N., and Gieseler, K. (2013). ZYX-1, the unique zyxin protein of Caenorhabditis elegans, is involved in dystrophin-dependent muscle degeneration. Mol. Biol. Cell *24*, 1232–1249. https://doi.org/10.1091/mbc.E12-09-0679.

33. Kamath, R.S., Fraser, A.G., Dong, Y., Poulin, G., Durbin, R., Gotta, M., Kanapin, A., Le Bot, N., Moreno, S., Sohrmann, M., et al. (2003). Systematic functional analysis of the Caenorhabditis elegans genome using RNAi. Nature *421*, 231–237. https://doi.org/10.1038/nature01278.

34. Whitfield, C.W., Bénard, C., Barnes, T., Hekimi, S., and Kim, S.K. (1999). Basolateral localization of the *Caenorhabditis elegans* epidermal growth factor receptor in epithelial cells by the PDZ protein LIN-10. Mol. Biol. Cell *10*, 2087–2100. https://doi.org/10.1091/mbc.10.6.2087.

35. Mello, C.C., Kramer, J.M., Stinchcomb, D., and Ambros, V. (1991). Efficient gene transfer in C.elegans: extrachromosomal maintenance and integration of transforming sequences. EMBO J. *10*, 3959–3970. https://doi.org/10.1002/j.1460-2075.1991.tb04966.x.

36. Maduro, M., and Pilgrim, D. (1996). Conservation of function and expression of unc-119 from two Caenorhabditis species despite divergence of non-coding DNA. Gene *183*, 77–85. https://doi.org/10.1016/s0378-1119(96)00491-x.

37. Brenner, S. (1974). The genetics of Caenorhabditis elegans. Genetics *77*, 71–94.

38. Dickinson, D.J., Pani, A.M., Heppert, J.K., Higgins, C.D., and Goldstein, B. (2015). Streamlined genome engineering with a self-excising drug selection cassette. Genetics *200*, 1035–1049. https://doi.org/10.1534/genetics.115.178335.

39. Schwartz, M.L., and Jorgensen, E.M. (2016). SapTrap, a toolkit for high-throughput CRISPR/Cas9 gene modification in Caenorhabditis elegans. Genetics *202*, 1277–1288. https://doi.org/10.1534/genetics.115.184275.

40. Mello, C., and Fire, A. (1995). DNA transformation. In Caenorhabditis elegans: Modern Biological Analysis of an Organism, H.F. Epstein, and D.C. Shakes, eds. (Academic Press).

41. Walston, T., Tuskey, C., Edgar, L., Hawkins, N., Ellis, G., Bowerman, B., Wood, W., and Hardin, J. (2004). Multiple Wnt signaling pathways converge to orient the mitotic spindle in early C. elegans embryos. Dev. Cell *7*, 831–841. https://doi.org/10.1016/j.devcel.2004.10.008.

42. Albertson, D.G. (1984). Formation of the first cleavage spindle in nematode embryos. Dev. Biol. *101*, 61–72. https://doi.org/10.1016/0012-1606(84)90117-9.

43. Leung, B., Hermann, G.J., and Priess, J.R. (1999). Organogenesis of the Caenorhabditis elegans intestine. Dev. Biol. *216*, 114–134. https://doi.org/10.1006/dbio.1999.9471.

44. Raich, W.B., Agbunag, C., and Hardin, J. (1999). Rapid epithelial-sheet sealing in the Caenorhabditis elegans embryo requires cadherin-dependent filopodial priming. Curr. Biol. *9*, 1139–1146. https://doi.org/10.1016/S0960-9822(00)80015-9.

45. Edelstein, A., Amodaj, N., Hoover, K., Vale, R., and Stuurman, N. (2010). Computer control of microscopes using μManager. Curr. Protoc. Mol. Biol. *Chapter 14*. . Unit14.20. https://doi.org/10.1002/0471142727.mb1420s92.

46. Edelstein, A.D., Tsuchida, M.A., Amodaj, N., Pinkard, H., Vale, R.D., and Stuurman, N. (2014). Advanced methods of microscope control using μManager software. J. Biol. Methods *1*, 10. https://doi.org/10.14440/jbm.2014.36.

47. Shao, X., Lucas, B., Strauch, J., and Hardin, J. (2019). The adhesion modulation domain of Caenorhabditis elegans alpha-catenin regulates actin binding during morphogenesis. Mol. Biol. Cell *30*, 2115–2123. https://doi.org/10.1091/mbc.E19-01-0018.

48. Freeman, G.H., and Halton, J.H. (1951). Note on an exact treatment of contingency, goodness of fit and other problems of significance. Biometrika *38*, 141–149.

49. Bolte, S., and Cordelières, F.P. (2006). A guided tour into subcellular colocalization analysis in light microscopy. J. Microsc. *224*, 213–232. https://doi.org/10.1111/j.1365-2818.2006.01706.x.

50. Maiden, S.L., Harrison, N., Keegan, J., Cain, B., Lynch, A.M., Pettitt, J., and Hardin, J. (2013). Specific conserved C-terminal amino acids of Caenorhabditis elegans HMP-1/α-catenin modulate F-actin binding independently of vinculin. J. Biol. Chem. *288*, 5694–5706. https://doi.org/10.1074/jbc.M112.438093.

51. Mayers, J.R., Fyfe, I., Schuh, A.L., Chapman, E.R., Edwardson, J.M., and Audhya, A. (2011). ESCRT-0 assembles as a heterotetrameric complex on membranes and binds multiple ubiquitinylated cargoes simultaneously. J. Biol. Chem. *286*, 9636–9645. https://doi.org/10.1074/jbc.M110.185363.

52. Stiernagle, T. (2006). Maintenance of C. elegans. WormBook, 1–11. https://doi.org/10.1895/wormbook.1.101.1.

53. Zhang, Y., Wang, X., Matakatsu, H., Fehon, R., and Blair, S.S. (2016). The novel SH3 domain protein Dlish/CG10933 mediates fat signaling in Drosophila by binding and regulating Dachs. eLife *5*, e16624. https://doi.org/10.7554/eLife.16624.

STAR★METHODS

KEY RESOURCES TABLE

REAGENT or RESOURCE	SOURCE	IDENTIFIER
Antibodies		
Mouse anti-GFP	Invitrogen	Cat#A11120
Rabbit anti-GFP	Invitrogen	Cat#A11122
Rabbit polycolonal anti-HMP-1	Callaci et al.[11]	N/A
Rabbit polycolonal anti-HMR-1	Callaci et al.[11]	N/A
Mouse monoclonal anti-ZYX-1	Lecroisey et al.[32]	N/A
Mouse monoclonal anti-AJM-1, MH27	Hardin lab ascites	N/A
Goat anti-rabbit IgG Texas Red	Invitrogen	Cat#T-2767
Goat anti-rabbit IgG FITC	Invitrogen	Cat#31635
Goat anti-mouse IgG Texas Red	Abcam	Cat#ab6787; RRID:AB_955583
anti-mouse FITC	Sigma-Aldrich	Lot#SLBZ0072
IRDye 680RD Goat anti-Rabbit IgG Secondary Antibody	Li-COR	Cat#926-68071; RRID:AB_10956166
IRDye 680RD Donkey anti-Mouse IgG Secondary Antibody	Li-COR	Cat#926-68072; RRID:AB_10953628
IRDye 800CW Goat anti-Rabbit IgG Secondary Antibody	Li-COR	Cat#926-32211; RRID:AB_621843
IRDye 800CW Donkey anti-Mouse IgG Secondary Antibody	Li-COR	Cat#926-32212; RRID:AB_621847
Bacterial and virus strains		
Escherichia coli OP50	CGC	N/A
Escherichia coli BL21-Gold (DE3)	Sigma-Aldrich	Cat#69450-M
Escherichia coli clone for C. elegans CDS B0496.8 (*tes-1*)	Ahringer library; Kamath et al.[33]	N/A
Escherichia coli clone for *C. elegans* CDS C10H11.9 (*let-502*)	Ahringer library; Kamath et al.[33]	N/A
Escherichia coli clone for *C. elegans* CDS C06C3.1 (*mel-11*)	Ahringer library; Kamath et al.[33]	N/A
Chemicals, peptides, and recombinant proteins		
Alexa Fluor 488 Phalloidin	Invitrogen	Cat#A12379
Alexa Fluor 660 Phalloidin	Invitrogen	Cat#A22285
ProTEV Plus	Promega	Cat#V6102
polymerized chicken F-actin	Cytoskeleton	Cat#AS99-B
T7 Megascript kit	ThermoFisher	Cat#AM1334
T3 Megascript kit	ThermoFisher	Cat#AM1338
Phusion DNA polymerase	ThermoFisher	Cat#F630S
Experimental models: Cell lines		
NIH 3T3 fibroblasts	American Type Culture Collection	CRL-1658
Mouse: Embryonic fibroblasts (MEFs)	Gibco	Cat#A34181
Experimental models: Organisms/strains		
C. elegans N2: wildtype	CGC	N2
C. elegans HR1157: *let-502(sb118ts)I*	Mains Lab	HR1157
C. elegans LP810: *zyx-1(cp415[mNG::zyx-1a])II*	Goldstein Lab	LP810
C. elegans LP831: *zyx-1Δ(cp419[Pmyo-2>GFP])II*	Goldstein Lab	LP831
C. elegans ML1651: *mcIs46 [dlg-1::RFP + unc-119(+)]*	Labouesse Lab	ML1651

(*Continued on next page*)

Continued

REAGENT or RESOURCE	SOURCE	IDENTIFIER
C. elegans MQ468: *hmp-2(qm39)I*	Hekimi Lab	MQ468
C. elegans PE532: *xnIs96[pJN455(hmr-1p::hmr-1::GFP::unc-54 3'UTR) + unc-119(+)]*	Pettitt Lab	PE532
C. elegans PE633: *feEx324[zyx-1::mCherry rol-6(su1006)]*	Pettitt Lab	PE633
C. elegans PE636: *feEx327[zyx-1::gfp Pmyo-2::dTomato]*	Pettitt Lab	PE636
C. elegans PE644: *zyx-1(gk190)II; feEx327[zyx-1::gfp myo-2p::dTomato]*	Pettitt Lab	PE644
C. elegans PE647: *zyx-1(gk190)II; hmp-1(fe4)/nT1V, feEx328[zyx-1D376-603::gfp myo-2p::dTomato]*	Pettitt Lab	PE647
C. elegans PE649: *zyx-1(gk190)II; hmp-1(fe4)/nT1V; feEx329[zyx-1D479-603::gfp myo-2p::dTomato]*	Pettitt Lab	PE649
C. elegans PE650: *zyx-1(gk190)II; hmp-1(fe4)/nT1V; feEx330[zyx-1D526-603::gfp myo-2p::dTomato]*	Pettitt Lab	PE650
C. elegans PE651: *zyx-1(gk190)II; hmp-1(fe4)/nT1V; feEx331[zyx-1D166-200::gfp myo-2p::dTomato]*	Pettitt Lab	PE651
C. elegans PE671: *mcIs46[dlg-1::RFP + unc-119(+)]; feEx327[zyx-1::gfp myo-2p::dTomato]*	Pettitt Lab	PE671
C. elegans PE97: *hmp-1(fe4)V*	Pettitt Lab	PE97
C. elegans PHX5560: *zyx-1(syb5560[mNG::zyx-1a, deltaLIM1-3])II*	This paper	PHX5560
C. elegans PHX5622: *tes-1(syb5622[mNG::FLAG::tes-1, deltaLIM1-3])IV*	This paper	PHX5622
C. elegans PHX5627: *tes-1(syb5622[mNG::FLAG::tes-1, deltaPET])IV*	This paper	PHX5627
C. elegans SU1042: *tes-1(jc71[mNeonGreen::tes-1])IV; zyx-1(gk190)II*	This paper	SU1042
C. elegans SU1043: *tes-1(jc71[mNeonGreen::tes-1])IV; mcEX40[plin-26::vab-10::mcherry; myo-2::gfp])IV*	This paper	SU1043
C. elegans SU1044: *tes-1(jc71[mNeonGreen::tes-1])IV; curIs[plin-26::lifeact::mcherry::unc-54 3'UTR; unc-119(+)]*	This paper	SU1044
C. elegans SU1058: *tes-1(jc71[mNG::tes-1])IV; zyx-1Δ(cp419[Pmyo-2>GFP])II*	This paper	SU1058
C. elegans SU1072: *tes-1(jc71[mNG::FLAG::tes-1])IV; hmp-1(jc58[hmp-1::mScarlet-I+LoxP511])V*	This paper	SU1072
C. elegans SU1073: *zyx-1Δ(cp419[Pmyo-2>GFP])II; tes-1(ok1036)IV*	This paper	SU1073
C. elegans SU1085: *tes-1(jc110[mScarlet-I::FLAG::tes-1+LoxP511])IV*	This paper	SU1085
C. elegans SU1087: *zyx-1(cp415[mNG::zyx-1a])II; curIs[plin-26::lifeact::mcherry::unc-54 3'UTR; unc-119(+)]*	This paper	SU1087
C. elegans SU1088: *zyx-1(syb5560[mNG::zyx-1a, deltaLIM1-3])II; curIs[plin-26::lifeact::mcherry::unc-54 3'UTR; unc-119(+)]*	This paper	SU1088
C. elegans SU1090: *tes-1(jc110[mScarlet-I::FLAG::tes-1+LoxP511])IV; zyx-1(syb5560[mNG::zyx-1a, deltaLIM1-3])II*	This paper	SU1090
C. elegans SU1091: *tes-1(jc110[mScarlet-I::FLAG::tes-1+LoxP511])IV; zyx-1(cp415[mNG::zyx-1a])II*	This paper	SU1091
C. elegans SU1094: *zyx-1(cp415[mNG::zyx-1a])II; tes-1(ok1036)IV*	This paper	SU1094
C. elegans SU1100: *zyx-1(gk190)II; curIs[plin-26::lifeact::mcherry::unc-54 3'UTR; unc-119(+)]*	This paper	SU1100

(*Continued on next page*)

Continued

REAGENT or RESOURCE	SOURCE	IDENTIFIER
C. elegans SU1101: *tes-1(syb5622[mNG::FLAG::tes-1, deltaLIM1-3])IV; curIs[plin-26::lifeact::mcherry:: unc-54 3'UTR; unc-119(+)]*	This paper	SU1101
C. elegans SU1107: *zyx-1Δ(cp419[Pmyo-2>GFP])II; tes-1(syb5622[mNG::FLAG::tes-1, deltaLIM1-3])IV*	This paper	SU1107
C. elegans SU496: *N2; jcEx159 [5kbptes-1::tes-1::gfp; pRF4; F35D3]*	This paper	SU496
C. elegans SU708: *N2; jcEx229[pRF4; Ptes-1::tes-1deltaPET::gfp F2-8; F35D3]*	This paper	SU708
C. elegans SU709: *N2; jcEx230[pRF4; Ptes-1::tes-1deltaPET::gfp F2-6; F35D3]*	This paper	SU709
C. elegans SU710: *N2; jcEx231[pRF4; Ptes-1::tes-1deltaLIM1::gfp; F35D3]*	This paper	SU710
C. elegans SU713: *N2; jcEx234[pRF4; Ptes-1::tes-1deltaLIM2::gfp F2-7; F35D3]*	This paper	SU713
C. elegans SU714: *N2; jcEx235[pRF4; Ptes-1::tes-1deltaLIM3::gfp; F35D3]*	This paper	SU714
C. elegans SU715: *N2; jcEx236[pRF4; Ptes-1::tes-1deltaLIM1-3::gfp; F35D3]*	This paper	SU715
C. elegans SU896: *hmp-1 (jc58[hmp-1::mScarlet-I + Lox511])V*	This paper	SU896
C. elegans SU931: *curIs[plin-26::lifeact::mcherry::unc-54 3'UTR; unc-119(+)]*	This paper	SU931
C. elegans SU955: *tes-1(jc71[mNG::FLAG::tes-1])IV*	This paper	SU955
C. elegans VC299: *zyx-1(gk190)II*	Moerman Lab	VC299
C. elegans VC696: *tes-1(ok1036)IV*	Moerman Lab	VC696
Oligonucleotides		
tes-1 N-terminal 5' Homology arm Forward Primer: GGCTGCTCTTCgTGGtttcttacctattttaaaatgacacctgcc	IDT	N/A
tes-1 N-terminal 5' Homology arm Reverse Primer: GGGTGCTCTTCgCATCATtactgaaattaattggcatttaacgct	IDT	N/A
tes-1 N-terminal 3' Homology arm Forward Primer: GGCTGCTCTTCgACGACCGACGTCACGTCTCCCGTTGTtGAC	IDT	N/A
tes-1 N-terminal 3' Homology arm Reverse Primer: GGGTGCTCTTCgTACGTCTGGAAGTGGTGCCCACGCATAC	IDT	N/A
tes-1 N-terminal sgRNA: GCACGGCTTCTCGTCCACAA	IDT	N/A
tes-1 2kb promoter amplify Forward Primer: GCGTCGACGAGTTTTTGTCAAGAGTAAGAC	IDT	N/A
tes-1 2kb promoter amplify Reverse Primer: GCCCCGGGATCAACTGATCATCCGGATTCG	IDT	N/A
tes-1 5kb promoter amplify Forward Primer: GCCTGCAGGAAGACAACGCTTGTCAAGAAT	IDT	N/A
tes-1 5kb promoter amplify Reverse Primer: GCGTCGACATTTTGCCCTCGAAATGCAATAC	IDT	N/A
Recombinant DNA		
cDNA yk662b10 (*hmr-1*)	NEXTDB, Kohara Lab	https://nematode.nig.ac.jp/doc/readme.php
cDNA yk285a2 (*ajm-1*)	NEXTDB, Kohara Lab	https://nematode.nig.ac.jp/doc/readme.php
cDNA yk1054c06 (*zyx-1*)	NEXTDB, Kohara Lab	https://nematode.nig.ac.jp/doc/readme.php
Plasmid: pPD95_75	Addgene	Addgene_1494
F35D3	Whitfield et al.[34]	N/A

(*Continued on next page*)

Continued		
REAGENT or RESOURCE	SOURCE	IDENTIFIER
pRF4 [*rol-6(su1006)* transgenic marker]	Mello et al.[35]	N/A
Cbr-unc-119(+)	Maduro et al.[36]	N/A
Pmyo-2::dTomato	Korswagen Lab	N/A
Plasmid: *Ptes-1(2kb)::tes-1::gfp*	This paper	pAML224
Plasmid: *Ptes-1(5kb)::tes-1::gfp*	This paper	pAML224v2
Plasmid: *SUMO-His-hmp-1*	Callaci et al.[11]	N/A
Software and algorithms		
Fiji	ImageJ	https://imagej.nih.gov/ij/
GraphPad Prism v.9.0	GraphPad	https://www.graphpad.com/scientific-software/prism/
Adobe illustrator	Adobe	https://www.adobe.com
Micromanager	Micromanager	https://micro-manager.org/
Fusion	Andor	https://andor.oxinst.com/downloads/view/fusion-release-2.3
Imaris	Imaris	https://imaris.oxinst.com/
QuickTime movie plugins for ImageJ	Hardin Lab	https://worms.zoology.wisc.edu/research/4d/4d.html
JACoP Plugins	ImageJ	https://imagej.nih.gov/ij/plugins/track/jacop.html

RESOURCE AVAILABILITY

Lead contact

Further information and requests for resources and reagents should be directed to and will be fulfilled by the lead contact, Dr. Jeff Hardin (jdhardin@wisc.edu).

Materials availability

All unique/stable reagents generated in this study are available from the lead contact upon request.

Data and code availability

- All data reported in this paper will be shared by the lead contact upon request.
- This paper does not report original code.
- Any additional information required to reanalyze the data reported in this paper is available from the lead contact upon request.

EXPERIMENTAL MODEL AND SUBJECT DETAILS

C. elegans strains were maintained on standard nematode growth medium plates seeded with OP50 *E. coli*[37] at either 15°C (temperature sensitive strains) or 20°C (all other strains). Bristol N2 was used as wildtype. Details of strains used in this study can be found in the key resources table.

NIH 3T3 fibroblasts (American Type Culture Collection, Manassas, VA) and mouse embryonic fibroblasts (MEFs) were cultured in DMEM media (Mediatech, Herndon, VA) and supplemented with 10% fetal bovine serum (HyClone; ThermoFisher Scientific, Hampton, NH), 2 mM L-glutamine (Invitrogen, Caarlsbad, CA) and penicillin–streptomycin (Invitrogen).

METHOD DETAILS

Molecular cloning

A ~5kb genomic sequence containing 2kb of the promoter and the entire genomic region of *tes-1* was PCR amplified using Phusion polymerase (ThermoFisher). The primers used were: 5' GCGTCGACGAGTTTTTGTCAAGAGTAAGAC and 3' GCCCCGGGAT CAACTGATCATCCGGATTCG. The PCR product was digested with *SalI* and *SmaI* and ligated into a similarly digested Fire lab vector pPD95.75, which contains the GFP sequence. A frameshift was repaired via PCR to generate a *Ptes-1(2kb)::tes-1::gfp* construct (pAML224). To generate *Ptes-1(5kb)::tes-1::gfp*, additional promoter sequence was PCR amplified using Phusion polymerase. The primers used were:

5' GCCTGCAGGAAGACAACGCTTGTCAAGAAT and 3' GCGTCGACATTTTGCCCTCGAAATGCAATAC. The PCR product and pAML224 were digested using *PstI* and *SalI* and ligated together to generate pAML224v2. The identity of pAML224v2 was confirmed via sequencing. Domain deletions were performed using circle PCR as described previously.[4]

CRISPR

mNG::TES-1 worms were generated via plasmid-based CRISPR/Cas9[38] using repair templates cloned using SapTrap cloning.[39] All domain deletion mutations (PHX strains) were generated by SunyBiotech (Fujian, China). Guides, homology arms primers, and single-stranded repair templates for all CRISPR/Cas9 editing can be found in the key resources table.

Microinjection

DNA was microinjected into worms as described previously.[40] Briefly, injection mixes consisting of 5ng/μl of transgenic *tes-1* DNA constructs, 20 ng/μl of junk DNA (F35D3[34]) and 75 ng/μl of pRF4 (*rol-6(su1006)* transgenic marker DNA)[35] were microinjected into both gonads of hermaphrodites. Progeny were screened for the presence of *rol-6(su1006)*, and stable lines were established by passaging of worms. For *zyx-1* transgenics, purified *zyx-1* deletion construct DNA (100ng/ml) was mixed with coinjection markers pRF4 (200ng/ml), *Cbr-unc-119*(+) (30ng/ml),[36] and *Pmyo-2::dTomato* (5ng/ml) (courtesy Rik Korswagen, Utrecht Univ.) diluted in sterile water. At least two stable lines from each injected transgene were used to analyze expression patterns.

Injection RNA interference was performed as described previously.[41] dsRNA was generated using ThermoFisher T7 and/or T3 Megascript kits; templates included Ahringer library[33] clones C10H11.9 (*let-502*) and C06C3.1 (*mel-11*), and Kohara clones yk662b10 (*hmr-1*), yk285a2 (*ajm-1*), and yk1054c06 (*zyx-1*) (NEXTDB, http://nematode.lab.nig.ac.jp/).

Antibody and phalloidin staining

Immunostaining was performed using freeze-cracking.[42] Staining was performed as described previously.[43] Embryos were mounted onto poly-L-lysine-coated ring slides and incubated with primary antibodies in PBST and 5% non-fat dry milk overnight at 4°C. Embryos were then incubated with secondary antibodies in PBST and 5% non-fat dry milk for approximately three hours at room temperature. The following primary antibodies were used: 1:1000 mouse-anti-GFP (Invitrogen), 1:1000 rabbit-anti-GFP, 1:4000 polyclonal rabbit-anti-HMP-1, 1:4000 polyclonal rabbit-anti-HMR-1 and 1:200 monoclonal mouse-anti-AJM-1 (MH27). The following secondary antibodies were used: 1:50 anti-rabbit IgG Texas Red, 1:50 anti-rabbit FITC, 1:50 anti-mouse Texas Red and 1:50 anti-mouse FITC.

Phalloidin staining of mutant and wild-type embryos was used to visualize actin in fixed embryos.[5] Embryos were mounted on poly-L-lysine-coated ring slides and fixed using the following: 4% paraformaldehyde, 0.1 mg/mL lysolecithin, 48 mM Pipes pH 6.8, 25 mM Hepes pH 6.8, 2 mM $MgCl_2$, and 10 mM EGTA for 20 minutes at room temperature. 1:20 Phalloidin-488 was incubated with embryos at room temperature for 90 minutes. Images of stained embryos were acquired as described below.

For co-immunostaining and phalloidin staining, embryos were gathered in a 1.5 mL Eppendorf tube and permeabilized with a solution of 4% paraformaldehyde, 10% Triton-X-100, 48 mM Pipes pH 6.8, 25 mM Hepes pH 6.8, 2 mM $MgCl_2$ and 10mM EGTA for 20 minutes at room temperature. Embryos were incubated overnight in PBST+5% dry milk+1:1000 rabbit-anti-GFP at 4°C on a nutator. Secondary antibodies (1:10 Phalloidin-660 and 1:50 anti-rabbit FITC) were incubated for 2 hours at room temperature. Images of stained embryos were acquired as described below.

DIC Imaging

Four dimensional DIC movies were gathered on either a Nikon Optiphot-2 connected to a QImaging camera or an Olympus BX5 connected to a Scion camera. Mounts were made as previously described.[44] QuickTime movie plugins for ImageJ (https://worms.zoology.wisc.edu/research/4d/4d.html) were used to compress and view movies.

Confocal microscopy

Spinning-disc confocal images of *tes-1* transgenics were acquired with a Z-slice spacing of 0.2μm for imaging of actin, 0.3μm for embryos stained for both GFP and actin, and 0.5μm for all other imaging using either Perkin Elmer Ultraview or Micromanager software[45,46] and a Nikon Eclipse E600 microscope connected to a Yokogawa CSU10 spinning disk scanhead and a Hamamatsu ORCA-ER charge-coupled device (CCD) camera. Junctional/cytoplasmic signal measurements were performed as described previously.[47] Fisher's exact test calculations were performed online at https://www.socscistatistics.com/tests/fisher/default2.aspx or using GraphPad Prism v. 9.0 software (GraphPad Software, San Diego, California, USA, www.graphpad.com). The extension of Fisher's exact test to a 4 x 2 contingency table[48] was performed online at https://vassarstats.net/fisher2x4.html. Other statistical analyses were performed using GraphPad Prism. For *zyx-1* transgenics, imaging was carried out using a Zeiss LSM 710 laser scanning confocal microscope equipped with 10x and 63x oil lenses.

For endogenous knock-ins, imaging was performed using a Dragonfly 500 spinning disc confocal microscope (Andor, Belfast, Ireland), mounted on a Leica DMi8 microscope, equipped with a Zyla camera and controlled by Fusion software (Andor). Images were collected using 0.18 μm slices with a 100×/1.3 NA oil immersion Leica objective at 20°C.

Colocalization analysis

Colocalization analysis was performed in Fiji using Just Another Colocalization Plugin (JACoP; https://imagej.nih.gov/ij/plugins/track/jacop.html).[49] 5 focal planes from >10 junctional segments were combined into single stacks for each genotype. Maximum

intensity Z projections were obtained, and automated Costes thresholding within JACoP was visually confirmed in each case. Significant difference in Pearson's R for colocalizations was assessed using the online Z calculator available at https://vassarstats.net/rdiff.html

Protein expression and purification

GST- and SUMO-His-tagged proteins were expressed in BL21-Gold (DE3) *Escherichia coli* cells and purified as described.[50,51] Cells were induced with 0.1mM IPTG at 18°C for 16 hours. Wash and elution buffers were as follows: GST wash (1X PBS, 500mM NaCl, 0.1% Tween-20, and 1mM DTT), GST elution (50mM Tris pH 8.0, 0.3% glutathione, 150mM NaCl), His wash (50mM Na-Phosphate pH 8.0, 300mM NaCl, 0.1% Tween-20, 10mM imidazole), and His elution (250mM imidazole, 100mM NaCl, 10% glycerol, 50mM Hepes pH 7.6). For actin-pelleting assays, the GST tag was cleaved from GST-TES-1 using ProTEV Plus (Promega), according to manufacturer's instructions.

Actin-Pelleting assays

Actin co-sedimentation assays were performed as described previously.[50] Briefly, 5μM purified, cleaved proteins (quantified via a Bradford Assay) were incubated at room temperature for one hour with 0 or 5μM polymerized chicken F-actin (Cytoskeleton). BSA was used a negative control, and SUMO-His-HMP-1[11] was used as a positive control. Samples were then centrifuged at 100,000 rpm for 20 min at 4°C in a TLA-120.1 rotor using a Beckman Optima tabletop ultracentrifuge. Samples were run on 12% SDS-PAGE gels, stained with Coomassie Brilliant Blue, and bands were quantified using ImageJ.

Co-immunoprecipitations and western blots

C. elegans expressing TES-1::GFP were grown in liquid culture as previously described.[52] Co-immunoprecipitations were completed as in Cox-Paulson et al.[31] Western blots were performed as described previously,[53] using rabbit anti-GFP, rabbit anti-HMP-1[11] and mouse anti-ZYX-1[32] primary antibodies and Li-COR IRDye secondary antibodies to detect proteins.

Stress fiber strain site assay

tes-1 and *zyx-1 LCR::mCherry* constructs were designed and expressed using the procedures described in detail by Winkelman et al.[2] Briefly, synthetic gBlock DNA encoding mammalian codon-optimized versions of the LIM1-3 domain of TES-1 and ZYX-1 were ordered from IDT (Coralville, Iowa), cloned into a CMV-driven expression vector that fused the C-termini of LCR(TES-1) and LCR(ZYX-1) to mCherry, and used to transfect zyxin $^{-/-}$ mouse embryo fibroblast cells (MEFs) rescued with stably integrated GFP-zyxin. Transfected MEFs were imaged on an inverted Nikon Ti-E microscope (Nikon, Melville, NY) with a Yokogawa CSU-X confocal scanhead and Zyla 4.2 sCMOS Camera (Andor, Belfast, UK). A 405 nm laser coupled to a Mosaic digital micromirror device (Andor) was used to locally damage stress fibers. Kymography was performed using ImageJ as described in Winkelman et al.[2]

QUANTIFICATION AND STATISTICAL ANALYSIS

Graphs were generated using GraphPad Prism. Unpaired Student's T-test or ANOVA was used to determine statistically significant differences between groups. Statistical test parameters, outcomes and reporting on number of samples used in each experiment are indicated in figure legends.

Current Biology, Volume *32*

Supplemental Information

TES-1/Tes and ZYX-1/Zyxin protect junctional actin networks under tension during epidermal morphogenesis in the *C. elegans* embryo

Allison M. Lynch, Yuyun Zhu, Bethany G. Lucas, Jonathan D. Winkelman, Keliya Bai, Sterling C.T. Martin, Samuel Block, Mark M. Slabodnick, Anjon Audhya, Bob Goldstein, Jonathan Pettitt, Margaret L. Gardel, and Jeff Hardin

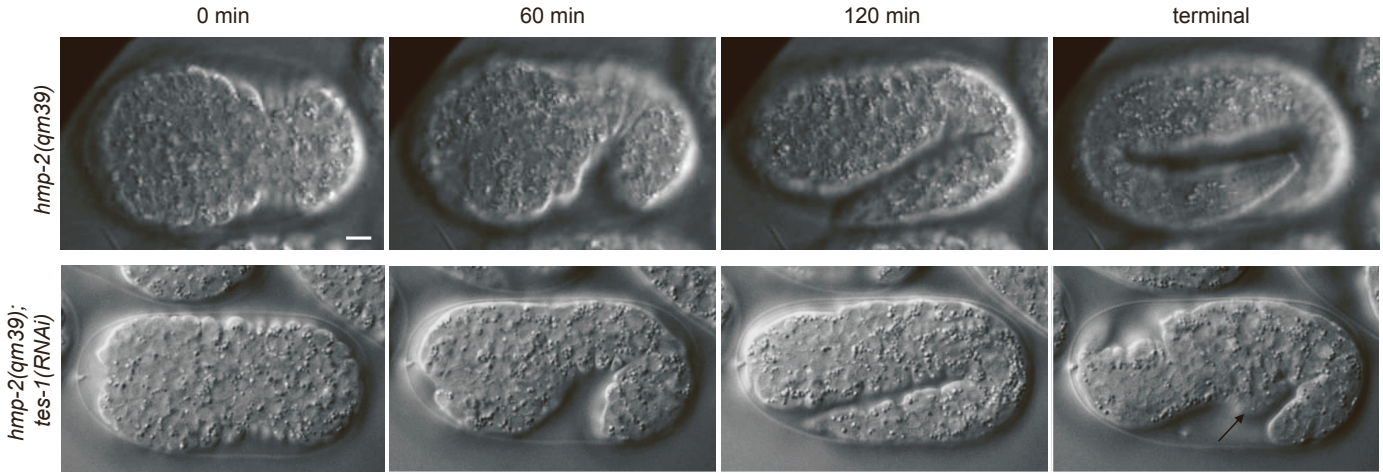
0 min
60 min
120 min
terminal
hmp-2(qm39)
hmp-2(qm39);
tes-1(RNAi)

Figure S1. Depletion of TES-1 enhances defects in a *hmp-2/β-catenin* hypomorph, Related to Figure 1 (Top) *hmp-2(qm39)* embryos are viable and display subtle body morphology defects. (Bottom) In *hmp-2(qm39); tes-1(RNAi)* embryos, cells leak out of the ventral midline in terminally arrested embryos (right panel, arrow). Scale bar = 5 μm.

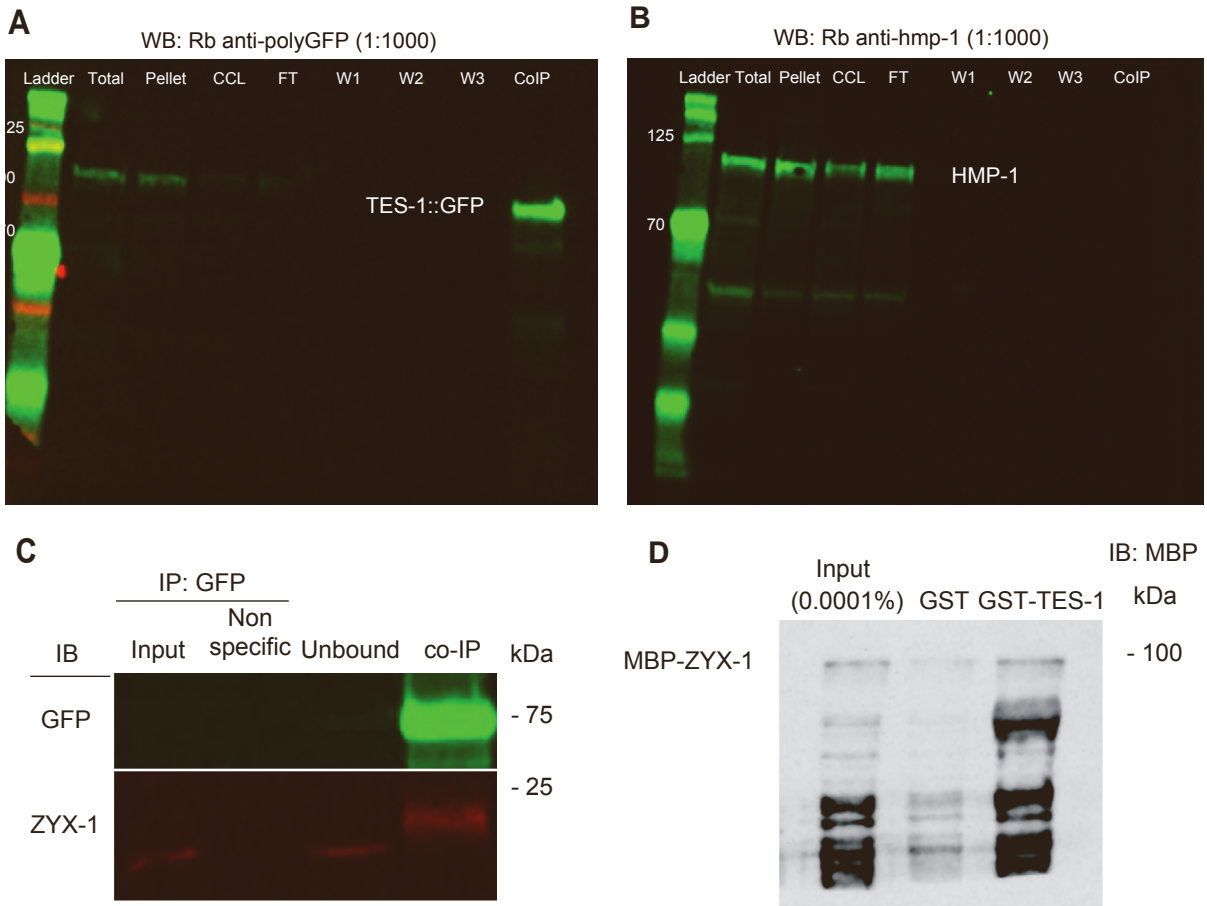
A
WB: Rb anti-polyGFP (1:1000)
Ladder
Total
Pellet
CCL
FT
W1
W2
W3
CoIP
TES-1::GFP
B
WB: Rb anti-hmp-1 (1:1000)
Ladder
Total
Pellet
CCL
FT
W1
W2
W3
CoIP
125
70
HMP-1
C
IP: GFP
IB
Input
Non specific
Unbound
co-IP
kDa
GFP
ZYX-1
- 75
- 25
D
IB: MBP
Input (0.0001%)
GST
GST-TES-1
kDa
MBP-ZYX-1
- 100

Figure S2. TES-1 binds weakly to ZYX-1/zyxin but cannot coimmunoprecipitate HMP-1/α-catenin, Related to Figure 2 and Figure 4 (A-B) TES-1::GFP was immunoprecipitated from an extract of mixed stage embryos, and the resulting proteins were blotted and probed with anti-GFP and anti-HMP-1 antibodies. (A) TES-1::GFP is substantially enriched in the IP fraction, demonstrating that anti-GFP antibodies can coIP TES-1::GFP. (B) Although in a parallel preparation HMP-1 can be detected in the total lysate, pellet and wash fractions, it is undetectable in the IP fraction. (C) Co-immunoprecipitation of TES-1 and ZYX-1. TES-1-GFP was immunoprecipitated from an extract of mixed stage embryos, and the resulting protein was blotted and probed with anti-GFP and anti-ZYX-1 antibodies. ZYX-1 is substantially enriched in the IP fraction. (D) Pulldown using recombinant ZYX-1/zyxin and TES-1/Tes. Extracts of bacteria expressing MBP-1-ZYX-1 were incubated with either GST or GST-TES-1. The resulting mixture was purified using glutathione beads, blotted, and probed using anti-MBP antibodies. MBP-ZYX-1 and TES-1-GST interact weakly at substoichiometric levels.

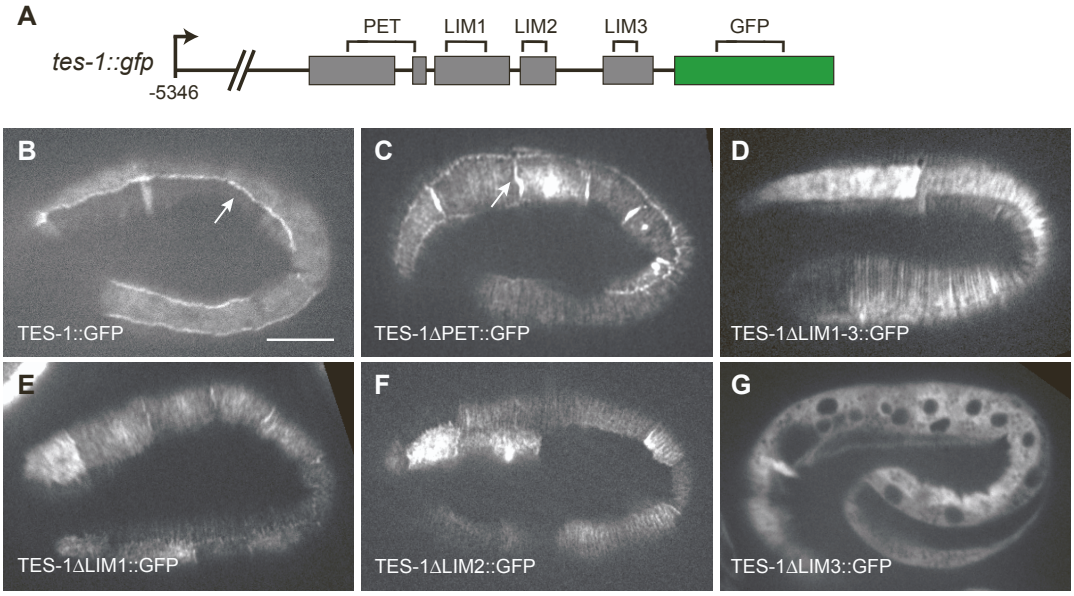

H

Transgene*	Lethal	Survival	% lethal
ok1036; fe4/+	30	46	39.5
+ ΔPET	24	98	19.7**
+ ΔLIM1-3	23	46	33.3
+ ΔLIM2	27	54	33.3
+ ΔLIM3	58	110	34.5

*Stable lines could not be recovered for ΔLIM1, see results
**Significantly different, $p<0.05$, Fisher's Exact Test

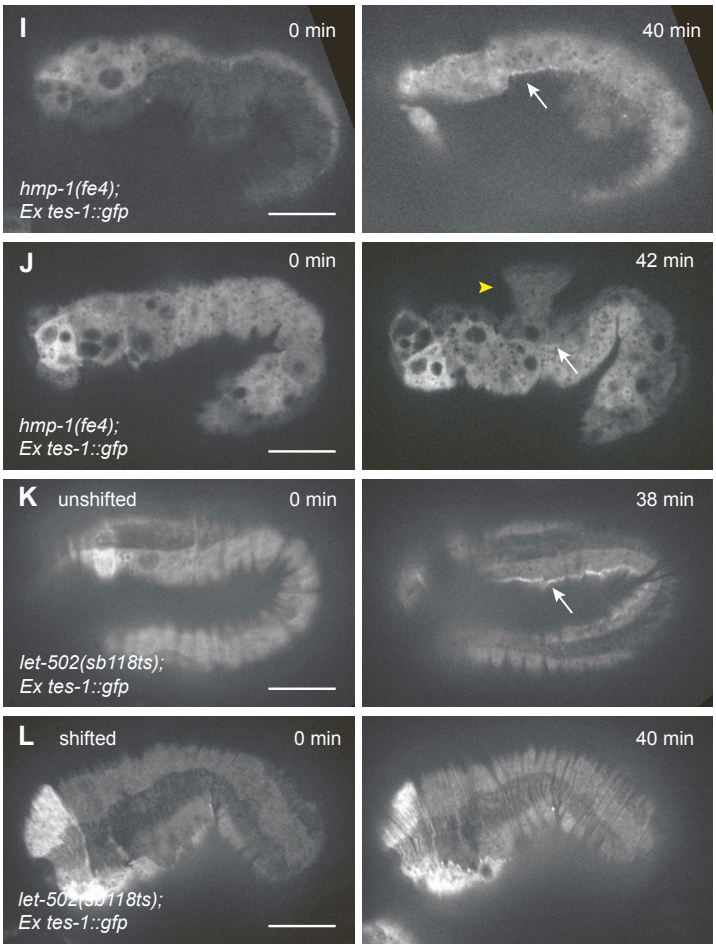

Figure S3. **TES-1 localization requires its PET and LCR domains, Related to Figure 3** (A) A schematic of the full-length TES-1::GFP driven by its full-length endogenous promoter used in this study. (B) Full-length TES-1::GFP localizes to dorsal-seam and ventral-seam cell boundaries in the epidermis (arrow). (C) Unlike full-length TES-1::GFP, TES-1ΔPET::GFP localizes along all seam cell borders in the epidermis, including seam-seam borders (arrows). (D) Deletion of all three LIM domains simultaneously results in GFP localization along structures that appear to be CFBs. Deletion of LIM1 (E) or LIM2 (F) both perturb junctional localization similarly: each localizes sporadically to epidermal junctions, including some seam-seam junctions. However, there is also localization at what appeared to be actin-containing structures in epidermal cells. (G) Deletion of LIM3 renders the GFP entirely cytoplasmic. (H) Rescue of embryonic lethality in progeny of *tes-1(ok1036); hmp-1(fe4)/+* hermaphrodites. * = significantly different from non-transgenic animals ($p < 0.05$, Fisher's exact test). (I) In *hmp-1(fe4)* embryos that successfully elongate to two-fold, TES-1::GFP accumulates along seam cell junctions (white arrow). (J) In *hmp-1(fe4)* embryos that do not elongate past 1.5-fold before failing, TES-1::GFP does not localize to junctions, instead remaining entirely cytoplasmic. Same embryo as Figure 3G. (K) In *let-502(sb118ts); tes-1::gfp* embryos reared at the permissive temperature ("unshifted"), development is normal and TES-1::GFP localizes to junctions as in wildtype. (L) In temperature-shifted embryos, the LET-502 protein is inactivated, embryos fail to elongate, and TES-1::GFP never accumulates along epidermal junctions. Same embryo as Figure 3H. Scale bars = 10 μm.

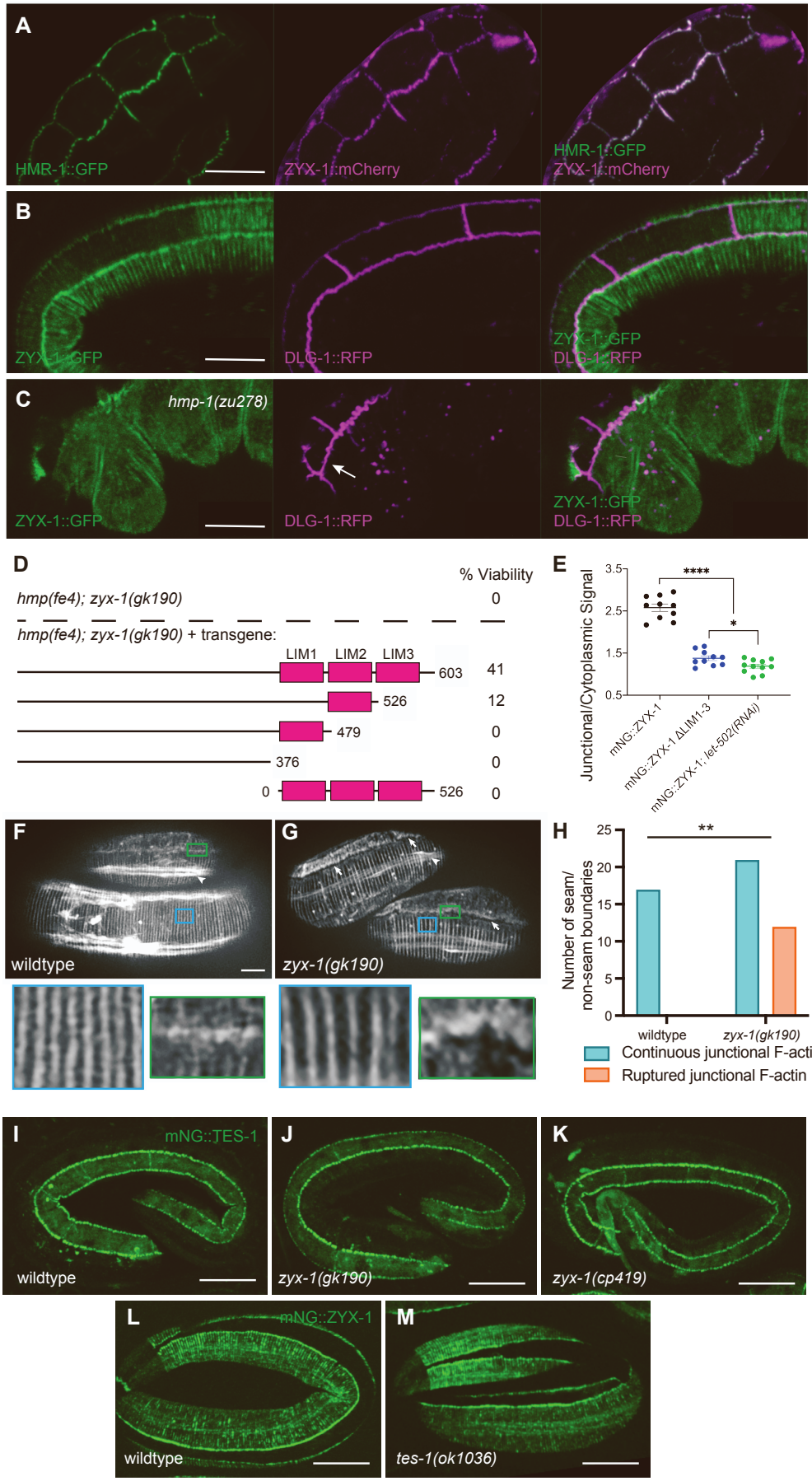
A
HMR-1::GFP
ZYX-1::mCherry
HMR-1::GFP
ZYX-1::mCherry
B
ZYX-1::GFP
DLG-1::RFP
ZYX-1::GFP
DLG-1::RFP
C
hmp-1(zu278)
ZYX-1::GFP
DLG-1::RFP
ZYX-1::GFP
DLG-1::RFP
D
% Viability
hmp(fe4); zyx-1(gk190)
0
hmp(fe4); zyx-1(gk190) + transgene:
LIM1
LIM2
LIM3
603
41
526
12
479
0
376
0
0
526
0
E
Junctional/Cytoplasmic Signal
3.5
2.5
1.5
0.5
****
*
mNG::ZYX-1
mNG::ZYX-1 ΔLIM1-3
mNG::ZYX-1; let-502(RNAi)
F
wildtype
G
zyx-1(gk190)
H
Number of seam/
non-seam boundaries
25
20
15
10
5
0
**
wildtype
zyx-1(gk190)
Continuous junctional F-actin
Ruptured junctional F-actin
I
mNG::TES-1
wildtype
J
zyx-1(gk190)
K
zyx-1(cp419)
L
mNG::ZYX-1
wildtype
M
tes-1(ok1036)

Figure S4. **ZYX-1 functions in a similar but independent manner as TES-1, Related to Figure 4** (A) Colocalization of HMR-1::GFP and ZYX-1::mCherry in otherwise wild-type embryos along a junctional boundary in seam cells during elongation. (B) Lack of colocalization of ZYX-1::GFP and DLG-1::RFP in otherwise wild-type embryos along a junctional boundary in seam cells during elongation. (C) Expression of ZYX-1::GFP and DLG-1::RFP in a *hmp-1(zu278)* homozygous embryo with the characteristic Humpback phenotype. DLG-1 localized to junctions in a superficial optical plane (arrows), but ZYX-1 does not. Scale bars = 5 μm. (D) Rescue of synthetic lethality in *hmp-1(fe4); zyx-1(gk190)* homozygotes by *zyx-1::gfp* transgenes (> 2000 progeny scores for each genotype). Full-length ZYX-1::GFP strongly rescues. (E) Junctional/cytoplasmic signal for mNG::ZYX-1 (n = 10 junctions), mNG::ZYX-1ΔLIM1-3 (n = 10), and mNG::ZYX-1; *let-502(RNAi)* embryos (n = 11). * = $p < 0.05$, **** = $p < 0.0001$, unpaired Student's T-test. (F-G) Fixed and phalloidin stained embryos. Bright staining is muscle (arrowhead). Scale bar = 5 μm. (F) Wild-type embryos exhibit parallel circumferential filament bundles (CFBs, blue box inset) and retain junctional-proximal actin (green box inset). (G) Some *zyx-1(gk190)* embryos exhibit ruptures in the junctional-proximal actin network (white arrows) although CFB organization looks normal. (H) Quantification of junctional proximal actin defects. Wildtype: n = 17 junctions; *zyx-1(gk190)*: n = 33; ** = $p < 0.01$, Fisher's exact test. (I-K) Junctional localization of mNG::TES-1 in (I) otherwise wild-type, (J) *zyx-1(gk190)*, and (K) *zyx-1(cp419[Pmyo-2>GFP])*, a CRISPR-induced null allele. There is no obvious disruption of TES-1 recruitment. (L-M) Junctional localization of mNG::ZYX-1A in (L) otherwise wild-type and (M) *tes-1(ok1036)* embryos. There is no obvious disruption of ZYX-1 recruitment. Scale bars = 10 μm.

Supplemental videos [available on the Hardin lab web site]

Video S1. *tes-1(RNAi)* enhances the severity of morphogenetic defects in *hmp-1(fe4)*embryos, related to Figure 1. Time lapse movie comparing *hmp-1(fe4)* homozygous and *hmp-1(fe4); tes-1(RNAi)* embryos. The latter fail consistently during early elongation, and all develop the Humpback phenotype. Time is shown in hours:minutes.
https://worms.zoology.wisc.edu/tes-1/video_s1.mp4

Video S2. Laser-induced recruitment of the ZYX-1 LCR::mCherry and mouse GFP::Zyxin to SFSS, related to Figure 4. Time lapse movie showing laser induction of a stress fiber strain site (SFSS) in a representative zyxin -/- mouse embryo fibroblast (MEF) rescued with stably integrated *M. musculus* GFP-zyxin and transiently transfected with a construct encoding ZYX-1 LCR::mCherry related to Figure 4D. White boxes show where light was targeted, and white arrows denote developing SFSS. Time is shown in minutes:sec.
https://worms.zoology.wisc.edu/tes-1/video_s2.mp4

Video S3. Laser-induced recruitment of the TES-1 LCR::mCherry and mouse GFP::Zyxin to SFSS, related to Figure 4. Time-lapse movie showing laser induction of a stress fiber strain site (SFSS) in a representative zyxin -/- mouse embryo fibroblast (MEF) rescued with stably integrated *M. musculus* GFP-zyxin and transiently transfected with a construct encoding TES-1 LCR::mCherry related to Figure 4F. White boxes show where light was targeted, and white arrows denote developing SFSS. Time is shown in minutes:sec.
https://worms.zoology.wisc.edu/tes-1/video_s3.mp4